Bioactive Materials 41 (2024) 108–126

Contents lists available at ScienceDirect

Bioactive Materials

journal homepage: www.keaipublishing.com/en/journals/bioactive-materials

Injectable citrate-based polyurethane-urea as a tug-of-war-inspired bioactive self-expansive and planar-fixing screw augmented bone-tendon healing

Meihan Tao [a], Zhou Fang [b], Yuting Zhu [b], Yan Ju [b], Zhiguo Hou [c], Meimei Fu [b], Zhihui Lu [b,c], Daozhang Cai [a,***], Jian Yang [d,**], Jinshan Guo [a,b,c,e,*]

[a] Department of Orthopedic Surgery, Guangdong Provincial Key Laboratory of Bone and Joint Degeneration Diseases, The Third Affiliated Hospital of Southern Medical University, Guangzhou, 510630, PR China
[b] Department of Histology and Embryology, NMPA Key Laboratory for Safety Evaluation of Cosmetics, School of Basic Medical Sciences, Southern Medical University, Guangzhou, 510515, PR China
[c] Regenerative Medicine and Tissue Repair Material Research Center, Huangpu Institute of Materials, Guangzhou New Materials Science Center, Changchun Institute of Applied Chemistry, Chinese Academy of Sciences, 88 Yonglong Avenue of Xinlong Town, Guangzhou, 511363, PR China
[d] Research Center for Industries of the Future, Biomedical Engineering Program, School of Engineering, Westlake University, Hangzhou, Zhejiang, 310030, PR China
[e] CAS Key Laboratory of High-Performance Synthetic Rubber and its Composite Materials, Changchun Institute of Applied Chemistry, Chinese Academy of Sciences, 5625 Renmin Street, Changchun, 130022, PR China

ARTICLE INFO

Keywords:
Polyurethane
Injectable
Self-expansive
Planar-fixing
Citrate

ABSTRACT

Inspired by tug-of-war, a game-changing bone-tendon fixation paradigm was developed. Specifically, injectable citrate-based bioactive self-expansive and planar-fixing screw (iCSP-Scr) consisting of reactive isocyanate (NCO) terminalized citrate-based polyurethane, proanthocyanidin modified hydroxyapatite (HAp) and water (with/without porogen) was developed and administrated in the bone-tendon gap. Instead of the "point to point" tendon fixation by traditional interface screws, along with the moisture-induced crosslinking and expansion of iCSP-Scr within the confined space of the irregularly shaped bone-tendon gap, the tendon graft was evenly squeezed into the bone tunnel in a "surface to surface" manner to realize strong and stable bone-tendon fixation via physical expansion, mechanical interlocking and chemical bonding (between –NCO and the $–NH_2$, –SH groups on bone matrix). The optimized iCSP-Scr exhibited rapid crosslinking, moderate expansion rate, high porosity after crosslinking, as well as tunable elasticity and toughness. The iCSP-Scr possessed favorable biodegradability, biocompatibility, and osteoinductivity derived from citrate, PC and HAp, it was able to promote osteogenesis and new bone growth inward of bone tunnel thus further enhanced the bone/iCSP-Scr mechanical interlock, ultimately leading to stronger tendon fixation (pull-out force 106.15 ± 23.15 N) comparing to titanium screws (93.76 ± 17.89 N) after 14 weeks' ACL reconstruction in a rabbit model. The iCSP-Scr not only can be used as a self-expansive screw facilitating bone-tendon healing, but also can be expanded into other osteogenic application scenarios.

1. Introduction

With an annual incidence rate of 68.6 per 100,000 person-years [1], anterior cruciate ligament (ACL) tear is one of the most common sports injuries, often leading to joint instability and dysfunction, cartilage and meniscus injury, osteoarthritis and even total knee arthroplasty [2,3]. ACL reconstruction, which can quickly restore most functions of the affected limb, has been established as the standard ACL injury repair surgery method for over 30 years [4–8]. Clinically, autologous, allogeneic, or artificial tendons used as ACL grafts are inserted into bone

Peer review under responsibility of KeAi Communications Co., Ltd.
* Corresponding author.
** Corresponding author.
*** Corresponding author.
E-mail addresses: daozhang@medmail.com.cn (D. Cai), yangjian07@westlake.edu.cn (J. Yang), jsguo4127@smu.edu.cn (J. Guo).

https://doi.org/10.1016/j.bioactmat.2024.07.004
Received 17 April 2024; Received in revised form 9 June 2024; Accepted 3 July 2024

tunnels established in the tibia and femur, then fixed to complete ACL reconstruction [5,8,9]. However, the prognosis of ACL reconstruction is not optimistic, with a failure rate of ~11.2% [10]; knee joint relaxation often occurs after surgery especially after resuming exercise, leading to secondary meniscus tear, cartilage injury, and even traumatic arthritis. Therefore, achieving effective bone-tendon fixation and healing is crucial in ensuring the success of ACL reconstruction.

Currently, the existing bone-tendon fixation methods suffer from various issues, such as stress concentration, uneven force distribution resulting in excessive tendon wear, or inadequate fixation. The fixation of tendons in bone tunnels mainly relies on the application of metal and polymeric interface/interference screws. Titanium [11], magnesium [12,13], and zinc [14] alloy screws are the main types of metal screws, with titanium screws the most commonly used due to their high initial fixation strength, corrosion resistance and cost-effectiveness. While, the mismatch in elastic moduli between metal screws and bone tissue often results in stress shielding effect, leading to local bone demineralization or impeding bone callus formation [15]. With favorable biocompatibility and similar elastic modulus to bone, polymeric screws, including non-degradable ones exemplified by polyetheretherketone (PEEK) screws [11] and bioresorbable/biodegradable ones such as poly(L-lactic acid) (PLLA)-based screws [4,16], have become widely accepted substitutes for metal screws in recent years. However, the fixation of tendon grafts within bone tunnel by either metal or polymeric screws is a punctiform fixation [11], often leads to stress concentration, excessive compression and uneven force distribution on the graft, and even graft rupture [11]. Without effective and tight bone-tendon fixation, lateral swing (windshield wiper effect) and longitudinal elongation (bungee jumping effect) always happen [11], induces tunnel enlargement and ultimately leads to ACL reconstruction failure. To address this issue, bone plugs (bone-tendon-bone autograft), suture anchors, metal plates with loop or cross pin systems have been developed [17], to assist interface/interference screws or function independently, facilitating better bone-tendon fixation. Up to now, the underlying mechanisms of bone-tendon fixation include compression (producing compressive loads to the longitudinal axis of tendon), expansion (generating a bulging of tendon) and suspension (suspending tendon into the bone tunnel) [17], with the compression mechanism being used the most frequently. Although significant progresses in the bone-tendon fixation technology have been made, issues like shape mismatch, as well as undesirable gaps between the fixation devices, grafts, and the bone tunnels still exist, an innovative strategy to realize better osteointegration and tighter bone-tendon fixation is urgently needed.

On the other hand, to improve bone-tendon healing efficacy and obtain better prognosis of ACL reconstruction, various regenerative medicine strategies have been developed. For example, periosteum [18] or magnesium pretreated periosteum [19], mesenchymal stem cells (MSCs) and their exosomes [20], platelet rich plasma [20,21], type I collagen/hydroxyapatite (HAp) patch [22], inorganic or composite bioactive bone cements/adhesives [23–25] and other biomaterials [26–28] have been used to topically apply on the implanted tendon grafts or modify the bone-tendon contact interface, resulting in enhanced bone-to-tendon healing performance. Biodegradable magnesium screws have been demonstrated to promote osteogenesis [13,29] and reduce peri-tunnel bone loss [12]. Similarly, zinc -based bone screws/implants have been reported to provide both antibacterial [30] and anti-osteolytic properties [14]. In addition to bioactive inorganic/metallic orthopaedic materials, due to the important bioactivity of citrate in bone and benefit from the versatile citrate chemistry platform, polymeric citrate-based biomaterials have also attracted considerable research attention [25,31–34]. As a key intermediate metabolite in the tricarboxylic acid (TCA) cycle, citrate is crucial for natural bone, with the skeletal system storing over 90% of the total citrate content in the body [34,35]. Citrate not only serves as a "controller" in regulating apatite nanocrystal structure [36], a "connector" between apatite and collagen [36], but also as an indispensable signaling molecule during "osteoblast citration" (osteoblasts are specialized citrate producing cells and produce citrate in bone formation) in osteogenic differentiation and mineralization [37]. Exogenous citrate derived from the degradation products of citrate-based biomaterials has been demonstrated to upregulate the bioenergy metabolism of MSCs in accommodating the initial high metabolic activity necessary during the osteogenic differentiation of MSCs [34]. It is worth to mention that the citrate-based (Citregen®) bone-tendon fixation medical devices, including interference screw (Citrelock™), knotless suture anchor (Citrefix™) and ACL implants (Citrespline™), have received the approval from the U.S. Food and Drug Administration (FDA) and are now being commercial implemented by Stryker. However, how to avoid the stress concentration caused by screws and balance the strong bioactivity of citrate and the mechanical stability essential in bone-tendon healing is still a significant challenge.

Herein, in order to solve the bone-tendon fixation problems such as uneven force distribution and inadequate fixation, inspired from the rope-grasping mode in tug-of-war, an innovative bone-tendon fixation paradigm was developed. By simply reacting oligomeric citrate-based polyol, poly(ε-caprolactone) (PCL) diol/triol, and N-methyldiethanolamine (MDEA) with excess diisocyanate (such as isophorone diisocyanate (IPDI)) in the presence of tin(II) bis(2-ethylhexanoate) ($Sn(OCt)_2$) as a catalyst, a reactive isocyanate (NCO) terminalized citrate-based polyurethane (CPU–NCO) was developed, which was further composited with proanthocyanidin (PC) modified HAp (PC-HAp) to form the injectable citrate-based polyurethane-urea as tug-of-war-inspired iCSP-Scr (Fig. 1A). When iCSP-Scr containing CPU-NCO/PC-HAp being injected in the narrow space between tendon graft and the bone in bone tunnel during ACL reconstruction, the residual –NCO groups immediately reacted with water (from body fluid or exogenously added) to produce $–NH_2$ groups and carbon dioxide (CO_2), thus tightly grasped the tendon graft in the bone tunnel through volume expansion during the solidification and crosslinking ration between –NCO and $–NH_2$ groups; the –NCO groups also can react with the available nucleophile groups ($-NH_2$, –SH) in peri-tunnel tissues to realize tissue adhesion, tight bone-tendon fixation was ultimately achieved through mechanical interlocking, physical expansion and chemical bonding (Fig. 1B and C). As one of the most effective antioxidants, PC was introduced to combat oxidant stress and modulate the inflammatory microenvironment [38]. On the other hand, the multiple phenolic hydroxyl groups and two aliphatic hydroxyl groups on PC might chemically react CPU-NCO thus bridge inorganic HAp and organic polymer [31]. The thermally reversible phenol-carbamate bond formed between the phenolic hydroxyl group in PC and –NCO also provided the possibility to speed up the degradation of iCSP-Scr [39,40]. The iCSP-Scrs with well-balanced performance were obtained by optimizing the proportions of different components. Subsequently, the physico-chemical properties, biocompatibility and osteogenic differentiation ability of the screws were evaluated *in vitro*. Finally, the bone-tendon healing efficacy of the iCSP-Scrs was further assessed in a rabbit ACL reconstruction model.

2. Materials and methods

2.1. Materials

Citric acid, tin(II) 2-ethylhexanoate ($Sn(OCt)_2$), hydroxyapatite (HAp) and polyethyleneglycol dimethyl ether (PEG-DM, Mn ~2000 Da) were all purchased from Sigma-Aldrich. Isophorone diisocyanate (IPDI, 99%, mixture of isomers), proanthocyanidin (PC), potassium hydroxide (KOH), toluene, ethanol and tris(hydroxymethyl) aminomethane hydrochloride (Tris-HCl) were from Macklin CO., Ltd. (Shanghai, China). MDEA and 1, 8-octanediol were purchased from Meryer CO., Ltd. (Shanghai, China). PCL diol ($M_n = 530$ Da) and PCL triol ($M_n = 370$ Da) were purchased from Daicel Technologies Co., Ltd. (Shanghai, China). All chemicals were used as received without any purification unless otherwise specified.

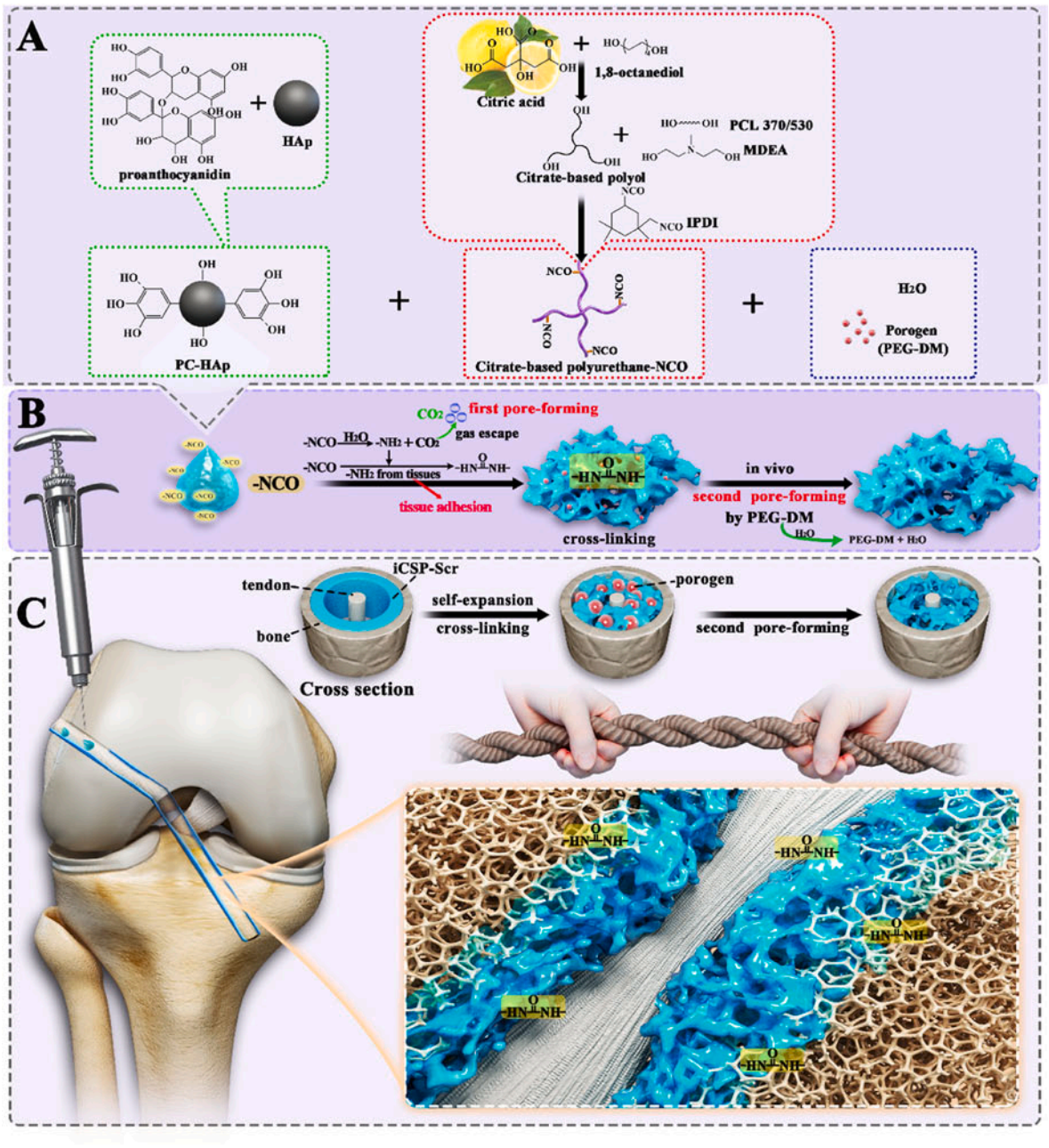

Fig. 1. The synthesis process of iCSP-Scr (A), the mechanism of iCSP-Scr expansion and pore formation (B), and the schematic diagram of using iCSP-Scr for ACL reconstruction (C). PCL370 represents PCL triol (Mn = 370 Da), PCL530 represents PCL diol (Mn = 530 Da), PEG-DM represents polyethyleneglycol dimethyl ether.

2.2. Synthesis of CPU-NCO and PC-HAp

By reacting citrate-based polyol, PCL diol/triol, and MDEA with excess IPDI, branched citrate-based polyurethane (CPU) capped with plenty unreacted terminal –NCO groups (CPU–NCO) was synthesized. Firstly, citrate-based polyol was obtained by reacting 19.21 g citric acid (0.10 mol) and 16.09 g 1, 8-octanediol (0.11 mol) at 140 °C for 2–3 h, and the acid value of the reaction mixture was monitored until it was stabilized at ~ 150 mg KOH/g.

Secondly, 11.25 g PCL diol (Mn = 530, 0.021 mol), 1.25 g PCL triol (Mn = 370, 0.00338 mol) and 2.50 g citrate-based polyol were mixed and stirred at 100 °C under vacuum for 3 h to remove water before reacting the mixture with 19.0 g IPDI (0.085 mol) at 60 °C under nitrogen atmosphere for 8 h. Then 1.01 g MDEA (0.0085 mol) was added and the reaction was continued with stirring for another 1 h, and 20.0 μg $Sn(OCt)_2$ was finally added to obtain CPU-NCO. The existence of terminal –NCO groups was characterized by Fourier transform infrared spectroscopy (FTIR) using a Thermo Fisher Scientific Nicolet iS50 FTIR spectrometer by casting CPU-NCO solution in anhydrous acetone on potassium bromide (KBr) slice, pure KBr slice was used as background. The crosslinked CPU (for 0.50 g CPU-NCO, 200 μL DI water was added) was characterized by attenuated total reflectance FTIR (ATR-FTIR, Thermo Fisher Scientific, iN10, USA), with air as background.

PC-HAp was synthesized by coating PC on the surface of HAp under slightly basic condition. Briefly, 2.0 g PC and 10.0 g HAp were added in 80 mL Tris-HCl buffer solution (0.1 M, pH 8.5), and stirred for 24 h at room temperature. Then the crude PC-HAp particles were collected via centrifugation at 5000 rpm for 10 min followed by washing with deionized (DI) water for at least three times. The purified PC-HAp was finally obtained after freeze-drying. ATR-FTIR was used to characterize HAp and PC-HAp.

2.3. Preparation and optimization of iCSP-Scr

The injectable citrate-based bioactive self-expansive and planar-fixing screw (iCSP-Scr) was obtained by uniformly mixing the designed amounts of CPU-NCO, PC-HAp, and water (with/without PEG-DM (as the porogen) in it), followed by the moisture initiated crosslinking process, until the system stopped expansion and solidified. For example, 0.5 g CPU-NCO was mixed with 0.1 g PC-HAp, then 200 μL H_2O containing 0.05 g PEG-DM was added, the uniformly mixed mixture was then allowed to set and solidify to give an iCSP-Scr named as CPU-$NCO_{0.5}$/PC-$HAp_{0.1}$ H_2O_{200}($P_{0.05}$) (P means porogen).

The injectable properties were evaluated through the video of writing with iCSP-Scr and the injection force test. The process of writing "SMU" using injectable iCSP-Scr was recorded by taking photos and videos (Fig. S1 and Video S1). The device for injection force test, as shown in Fig. S2 A, consisted of a tubular metal for fixing the syringe, a 5 mL syringe (without the needle), and an Instron 34TM-10 machine operating in compression mode equipped with a 500 N load cell. The newly synthesized iCSP-Scr was filled into a 5 mL syringe and then ejected by pushing the plunger downwards at a constant speed of 8 mm/min. The stable compression forces of at least 8 specifications after pushing down 0.5 mm were recorded and averaged to obtain the injection force.

The setting time was defined as the time required for iCSP-Scr to expand to the maximum volume from the uniform mixing of different components. Full solidification of iCSP-Scr took longer time; after 24 h, the hardness of iCSP-Scr stabilized, indicating the completion of crosslinking.

The crosslinking of iCSP-Scrs was conducted under different conditions, including free expansion on a flat surface and in a confined space (5 mL syringes and 2 mL plastic tubes with caps). To optimize the formulation of iCSP-Scr, the iCSP-Scrs with different formulations were crosslinked in 5 mL syringes. And to avoid possible ejection of the plug of the syringe under the high air pressure, several small holes were created on the bottom of the syringe. The influence of different component ratios of CPU-NCO, PC-HAp, H_2O and porogen to the expansion rates, porosity, mechanical strengths, and hardness of the obtained iCSP-Scrs was thoroughly investigated. The nomenclature of iCSP-Scrs with different formulations and the corresponding data for the tested indices were shown in Table 1. For each sample, 5 specimens were tested and the results were averaged, and were shown in Table 1 and Fig. 3. The iCSP-Scr with balanced performance, CPU-$NCO_{0.5}$/PC-$HAp_{0.1}$ H_2O_{200}($P_{0.05}$), was chosen as the representative for subsequent experiments.

At the same time, to simulate the incompletely sealed confined space of the bone tunnel in ACL reconstruction, iCSP-Scr (using the formulation CPU-$NCO_{0.5}$/PC-$HAp_{0.1}$ H_2O_{200}($P_{0.05}$) as representative) was also crosslinked in 2 mL tubes with the caps sealed (the sample was denoted as "Sealed"), with caps open (Open), with capped sealed but 3 holes were created in fixed positions on the bottom of each tube (Holes), or with the amount iCSP-Scrs doubled and the caps sealed and 3 holes created (Squeezed) (Fig. 2A and Table S2). The setting times, expansion rates, mechanical strengths and the degradation profiles of the obtained iCSP-Scr cylinders were studied.

2.4. Characterizations of iCSP-Scr

2.4.1. Expansion rate measurement

To facilitate quantitative detection of the volume of iCSP-Scr before and after expansion, 5 mL syringes and small NaCl salt particles filtered through a 120-mesh sieve (<125 μm) were used for testing. Specifically, in a 5 mL syringe, all components of an iCSP-Scr formulation were evenly mixed and compacted by the syringe to remove air, and the volume scale (V_{mix}) was recorded. After 24 h, the crosslinked iCSP-Scr solid was removed from the syringe and placed in a new syringe. The surrounding area of the solid was filled with the salt particles until the scale value of 5 mL. Then the salt particles were collected in another new syringe and the volume scale of the salt (V_{salt}) was recorded (Fig. S3). The expansion rate was calculated using Equation (1). For each sample, at least 5 specimens were tested and the results were averaged.

$$\text{Expansion rate}\ (\%) = (5 - V_{salt}) / V_{mix} \times 100 \quad (1)$$

2.4.2. Morphology observation and porosity measurement

The morphology and microstructure of the crosslinked iCSP-Scrs were observed using both stereomicroscope (SOPTOP SZX12, Running Optics, China) and scanning electron microscopy (SEM, ZEISS Sigma 300, Germany).

The porosity of the crosslinked iCSP-Scr was measured with the volumetric method [41]. The tested samples were cut into cubes (5 mm × 5 mm × 5 mm) and completely immersed in a measuring cylinder filled with 5 mL DI water, then the system was sealed and shaken for 10 min until no bubbles escaped from the samples any more. The porosity was calculated using formula (2).

$$\text{Porosity}\ (\%) = V_{pore} / V_{sample} \times 100 = (W_1 - W_0) / (\rho \times V_{sample}) \times 100 \quad (2)$$

Here, W_0 is the original weight (g) of the sample, W_1 represents the weight (g) of the sample after immersing in DI water for 10 min, and ρ is the density of DI water (1.0 g/cm^3). V_{sample} represents the total volume of the crosslinked iCSP-Scr cube. At least 5 specimens were tested for each sample and the results were averaged.

2.4.3. Rheological and mechanical property study

The rheological properties of the iCSP-Scr were evaluated with Rheometer (HAAKE MARS40, Germany) at 25 °C. Around 1 mL newly

Table 1
The nomenclature of iCSP-Scrs with different formulations and the corresponding data for the tested indices.

Variable	Sample	Expansion rate (%)	Porosity (%)	Compression strength (MPa)	Young's modulus (MPa)	Hardness (HA)
Water	CPU-$NCO_{0.5}$/PC-$HAp_{0.1}$ $H_2O_{\mathbf{50}}$(P_0)	335.0 ± 33.54	47.3 ± 1.49	42.5 ± 8.22	51.3 ± 12.04	/
	CPU-$NCO_{0.5}$/PC-$HAp_{0.1}$ $H_2O_{\mathbf{100}}$(P_0)	494.8 ± 31.87	63.5 ± 2.92	11.4 ± 1.25	28.5 ± 3.74	83.4 ± 6.11
	CPU-$NCO_{0.5}$/PC-$HAp_{0.1}$ $H_2O_{\mathbf{200}}$(P_0)	488.3 ± 38.72	63.6 ± 2.55	10.9 ± 3.12	30.8 ± 8.38	87.4 ± 2.07
	CPU-$NCO_{0.5}$/PC-$HAp_{0.1}$ $H_2O_{\mathbf{300}}$(P_0)	333.7 ± 76.35	52.7 ± 1.25	10.8 ± 1.67	27.4 ± 10.15	83.2 ± 7.89
PC-HAp	CPU-$NCO_{0.5}$/PC-$HAp_{\mathbf{0}}$ H_2O_{200}(P_0)	785.0 ± 33.54	85.7 ± 1.47	4.7 ± 0.66	12.3 ± 6.13	67.8 ± 0.84
	CPU-$NCO_{0.5}$/PC-$HAp_{\mathbf{0.1}}$ H_2O_{200}(P_0)	488.3 ± 38.72	62.0 ± 3.05	8.6 ± 1.56	27.6 ± 8.13	87.4 ± 1.14
	CPU-$NCO_{0.5}$/PC-$HAp_{\mathbf{0.2}}$ H_2O_{200}(P_0)	229.0 ± 33.24	34.2 ± 1.57	16.7 ± 4.62	45.0 ± 11.51	95.8 ± 1.92
HAp	CPU-$NCO_{0.5}$/$HAp_{\mathbf{0}}$ H_2O_{200}(P_0)	785.0 ± 33.54	85.4 ± 1.91	4.7 ± 0.66	12.3 ± 6.13	67.8 ± 0.84
	CPU-$NCO_{0.5}$/$HAp_{\mathbf{0.1}}$ H_2O_{200}(P_0)	460.0 ± 30.28	62.8 ± 1.47	9.9 ± 2.62	26.0 ± 7.41	80.2 ± 1.79
	CPU-$NCO_{0.5}$/$HAp_{\mathbf{0.2}}$ H_2O_{200}(P_0)	296.7 ± 36.13	43.0 ± 1.44	17.0 ± 3.99	45.0 ± 14.28	90.4 ± 1.14
Porogen	CPU-$NCO_{0.5}$/PC-$HAp_{0.1}$ H_2O_{200}($P_{\mathbf{0}}$)	421.3 ± 53.16	62.1 ± 1.88	7.5 ± 0.32	37.9 ± 4.89	87.8 ± 1.64
	CPU-$NCO_{0.5}$/PC-$HAp_{0.1}$ H_2O_{200}($P_{\mathbf{0.05}}$)	462.7 ± 44.37	64.7 ± 2.32	6.9 ± 1.48	32.1 ± 5.80	86.6 ± 2.30
	CPU-$NCO_{0.5}$/PC-$HAp_{0.1}$ H_2O_{200}($P_{\mathbf{0.1}}$)	496.0 ± 71.27	66.0 ± 2.28	6.1 ± 1.10	30.5 ± 3.71	83.4 ± 1.67

The different components are aligned in the order of CPU-NCO/PC-HAp H_2O(P), for example, CPU-$NCO_{0.5}$/PC-$HAp_{0.1}$ $H_2O_{\mathbf{50}}$($P_{0.1}$) is composed by 0.5 g CPU-NCO, 0.1 g PC-HAp, and 50 μL water (H_2O) containing 0.1 g porogen (PEG-DM).

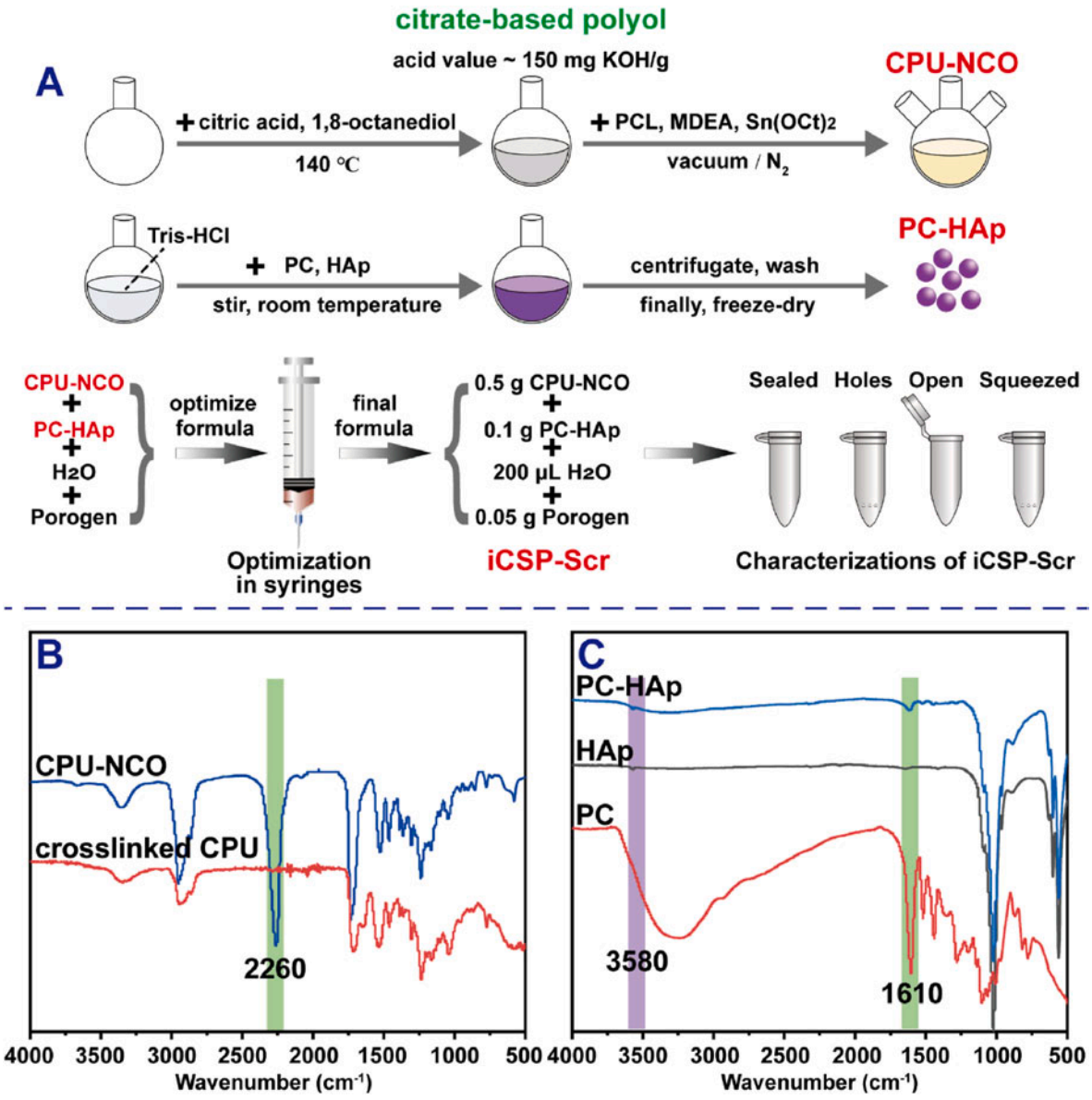

Fig. 2. The specific synthesis routes, optimization, and characterization process of iCSP-Scr (A), and the FTIR spectrum results of CPU before and after crosslinking (B) and HAp before and after modification (C).

synthesized iCSP-Scr was put in a parallel plate configuration (20 mm in diameter and 1 mm gap), the storage modulus (G′) and loss modulus (G″) were measured. A frequency of 1 Hz and 1% strain were applied to minimize possible interference to the gelation process and to keep the measurement within the linear viscoelastic region.

The mechanical properties, including the compression performance and the hardness of the crosslinked iCSP-Scrs at different conditions (Sealed, Open, Holes, Squeezed), were studied. For compression strength study, the crosslinked iCSP-Scrs were cut into cylinders (Φ6 mm × 12 mm) and compressed using an Instron 34TM-10 machine equipped with a 500 N load cell at a compression rate of 0.5 mm/min until the strain reached 70%. The Young's modulus was determined by the slope of the stress-strain curve from 0 % to 1% elongation. At least 5 specimens were tested for each sample and the results were averaged. For the hardness tests, the crosslinked iCSP-Scr was cut into cubes (5 mm × 5 mm × 5 mm) and their hardnesses were measured with a Shore hardness tester (LX-A, Wenzhou, China). When the result was greater than 90 HA, the hardness was measured using a LX-D Shore hardness tester instead. At least 5 specimens were tested for each sample and the results were averaged.

The adhesion property of iCSP-Scr was exhibited by a lap-shear test using wet porcine skin. Briefly, fresh porcine skin was cut into rectangular strips with 80 mm in length and 15 mm in width, and the oil on the skin was removed. The ends of two porcine skin pieces were applied with iCSP-Scr and then overlapped to form a lap shear joint, and then subjected to a curing process at 37 °C and 50% humidity for 2 h. Then one side of the adhered porcine skin was held and hung in the air to take photos. The porcine skin was also perforated and a 200 g metal weight was fixed to the porcine skin using cotton thread to further demonstrate the adhesion performance of iCSP-Scr.

2.4.4. *In vitro* biomechanical property

To simulate the tendon fixation effect of iCSP-Scr in ACL reconstruction *in vitro*, woven nylon rope was used as the tendon substitute and was fixed in 8 mm bone tunnel created in the femoral end of the pig's knee joint, and then pull-out tests were conducted. The control group was fixed with 8 mm titanium screws (Natton, Beijing, China), while the experimental group was evenly applied with iCSP-Scr injected

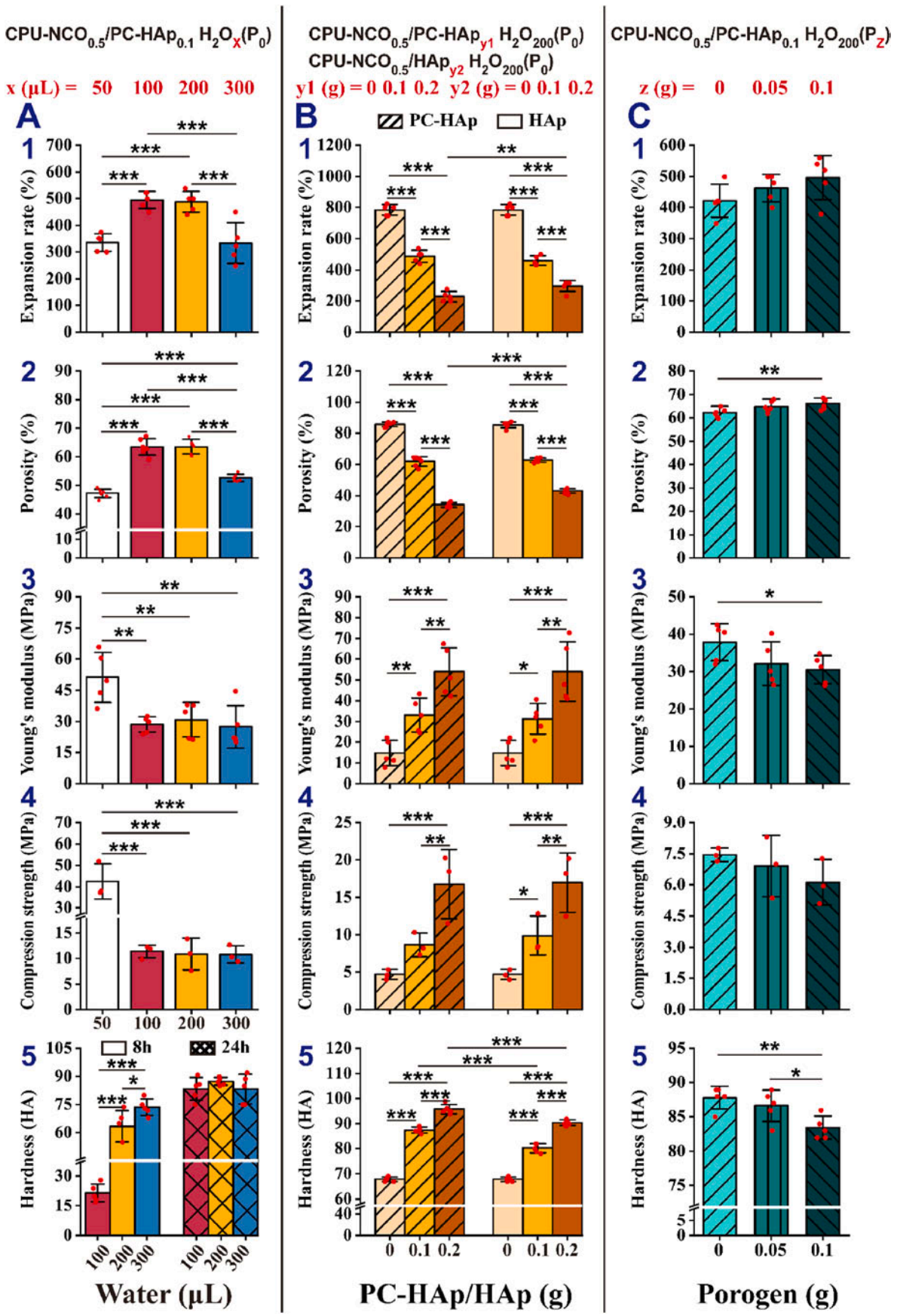

Fig. 3. The effect of different formulations (CPU–NCO/PC-HAp H_2O(porogen)) on the performance of iCSP-Scrs. *, **, and *** represent $p < 0.05$, $p < 0.01$ and $p < 0.001$, respectively.

in the bone tunnel. The bones were placed in the well mixed mixture of denture base materials (New Century, Shanghai, China) and prepared into a regular shape that was easy to grip (Fig. 5E). After 24 h at room temperature, the pull-out resistance strength was measured using Instron 34TM-10 machine equipped with a 10 kN load cell at a load displacement rate of 5 mm/min. The fixed tendon substitute of each specimen was aligned parallel to the two vertical beams of the Instron 34TM-10 machine, and pulled until the tendon substitute broke or was pulled out, to obtain the ultimate load to failure. At least 10 specimens were tested in each group, and the results were averaged.

2.4.5. Degradation and PC release profiles

The biodegradability of iCSP-Scr was evaluated *in vitro* at 37 °C in phase buffered saline (PBS, pH 7.4). Specifically, the crosslinked iCSP-Scr was cut into disc-shaped samples (diameter = 9 mm, 0.05 ± 0.005 g), accurately weighed (W_0), immersed in a capped tube containing 10 mL PBS, and incubated in a constant temperature oscillation incubator at 37 °C. At the predetermined time points, the samples were taken out, washed at least 3 times with pure DI water, freeze-dried and weighed (W_t). The mass loss rate was calculated according to equation (3).

$$\text{Mass loss}\ (\%) = (W_0 - W_t) / W_0 \times 100 \quad (3)$$

At the same time, the release of PC in PBS obtained after different degradation times was measured using a UV–vis spectrophotometer (Shimadzu, UV-2600). At least 5 specimens were tested for each sample at each time-point, and the results were averaged.

2.5. Biocompatibility of iCSP-Scr in vitro

2.5.1. Preparation of iCSP-Scr samples and degradation products

The iCSP-Scr prepared from PC-HAp (abbreviated as iCSP-Scr^P) was obtained by fully mixing and solidifying 0.5 g CPU-NCO, 0.1 g PC-HAp, and 200 μL water containing 0.05 g PEG-DM. The unmodified HAp iCSP-Scr (iCSP-Scr^H) used 0.1 g HAp to replace PC-HAp, with the other components being kept same as iCSP-Scr^P. The crosslinked iCSP-Scr^P and iCSP-Scr^H were cut into 0.01 g and 0.005 g pieces and sterilized with 5 kGy gamma ray irradiation for subsequent experiments.

To prepare the degradation products, 0.50 g crosslinked iCSP-Scr^P and iCSP-Scr^H samples were cut into pieces, immersed in 50 mL 2 M NaOH solution, incubated in a constant temperature oscillation incubator at 37 °C for 91 days, and the samples were partially degraded. The supernatant was collected and the pH was neutralized with concentrated hydrochloric acid, disinfected by passing through a 0.22 μm filter to obtain 1 × degradation product. Then the 1 × degradation product was further diluted 10 times and 100 times with sterile α-Minimal Essential Medium (α-MEM, Gibco, USA) to obtain the 10 × and 100 × degradation products.

2.5.2. Cytocompatibility assessment

Rat bone mesenchymal stem cells (BMSC, Cyagen, passage 4–6) were used to evaluate the cytotoxicity of iCSP-Scr through Cell Counting Kit-8 (CCK8, Vazyme, China) and Live/Dead staining. The complete medium for cell culture was prepared with α-MEM, 10% FBS (Gibco, USA) and 1% penicillin/streptomycin (Gibco, USA). The BMSC suspension in complete α-MEM at with a density of 4×10^4 cells/mL were seeded in 96 well plates for 100 μL per well. After the cells being cultured at 37 °C under 5 % CO_2 and 95 % relative humidity for 24 h in incubator, the medium was replaced by 90 μL fresh complete α-MEM, and 10 μL α-MEM, 1 × , 10 × or 100 × degradation products was also added. Cells cultured in pure complete α-MEM was set as control. After 1, 3, and 5 days in incubator, CCK8 assay was conducted to test the cytotoxicity by measuring the absorbance at 450 nm with an Epoch™ microplate spectrophotometer (BioTek, USA). Three independent experiments were conducted, and for each time point and each sample, at least three parallels were set, the results were then averaged (n = 3).

For Live/Dead staining, the complete medium of 100 × degradation product of iCSP-Scr^P (DP) was composed of 0.9 mL α-MEM, 0.1 mL 100 × DP, 10% FBS and 1% penicillin/streptomycin. BMSCs were seeded in 12 well plates at a density of 4×10^4 cells/mL and 1 mL/well. After 24 h' incubation, 12 wells were divided into 4 groups, by replacing the medium with 1.0 mL pure complete α-MEM (Control), 1.0 mL complete α-MEM + iCSP-Scr^P piece (0.01 g, iCSP-Scr^P), 1.0 mL complete α-MEM + iCSP-Scr^H piece (0.01 g, iCSP-Scr^H), and 1.0 mL complete medium of 100 × degradation product of iCSP-Scr^P (DP), respectively. After 24 and 48 h of cultivation, Live/Dead staining solution (Bestbio, China) was added, and the stained cells were then observed and photographed by an inverted fluorescent microscope (Olympus CKX41, Tokyo, Japan). The numbers of live and dead cells were also counted by image J. Three independent experiments were conducted (n = 3), and the representative results were used.

2.5.3. Cell migration study

The effect of iCSP-Scr to the cell migration capability was evaluated by scratch assay with iCSP-Scr^P, iCSP-Scr^H and the 100 × degradation product of iCSP-Scr^P. The α-MEM medium used in this study contained 2% FBS and 1% penicillin/streptomycin. And the complete medium of 100 × degradation product of iCSP-Scr^P (DP) was composed of 0.9 mL α-MEM, 0.1 mL 100 × DP, 2% FBS and 1% penicillin/streptomycin. The BMSCs were seeded in 12 well plates with a density of 1×10^4 cells/well with 1.0 mL medium per well. After 24 h, three parallel scratches were created using a 1000 μL pipette tip, the floating cells was washed with sterile PBS (pH 7.4) for three times, and then α-MEM (abbreviated as "Control"), α-MEM + iCSP-Scr^P piece (1.0 mL/0.01 g, abbreviated as "iCSP-Scr^P"), α-MEM + iCSP-Scr^H piece (1.0 mL/0.01 g, abbreviated as "iCSP-Scr^H"), and the 100 × degradation product of iCSP-Scr^P (1.0 mL complete medium of 100 × DP, abbreviated as "DP") were added. After 0 and 24 h, the cells were observed and photographed by an inverted fluorescent microscope (Olympus CKX41, Tokyo, Japan), and the cell migration rate was quantitatively calculated by Image J using Equation (4).

$$\text{Migration rate}\ (\%) = (A_0 - A_{24}) / A_0 \times 100 \quad (4)$$

Here, A_0 represents the initial scratch area at 0 h, A_{24} represents the scratch area after 24 h' incubation, n = 4.

2.5.4. Cell adhesion and growth on iCSP-Scr

To evaluate the cell adhesion and growth on iCSP-Scr, cells were seeded on the crosslinked iCSP-Scr ($CPU–NCO_{0.5}$/$PC\text{-}HAp_{0.1}$ $H_2O_{200}(P_{0.05})$), the adhesion of fluorescence labeled (by Calcein AM, for alive cells) cells on the material surface was observed using a laser scanning confocal microscope (LSCM, Carl Zeiss, Germany), and the microstructure was also observed by SEM (ZEISS Gemini 300, Germany). In the preliminary experiment, it was found that the crosslinked iCSP-Scr can be stained by 4', 6-diamidino-2-phenylindole (DAPI). Therefore, the cell was stained green by Calcein AM (Bestbio, China), and the material and nucleus were stained blue by DAPI (Solarbio, China) before LSCM observation. For SEM study, the cells were fixed by 4% paraformaldehyde (Biosharp, China) followed by gradient dehydration and sputter coating with gold before SEM observation.

2.6. In vitro osteogenic properties of iCSP-Scr against BMSCs and tendon derived cells (TDCs)

2.6.1. Preparation of osteogenic medium

The osteogenic (OG) medium was composed of complete α-MEM (Gibco, USA) medium containing 10% FBS (Gibco, USA) and 1% penicillin-streptomycin (Gibco, USA), with 10 nmol/L dexamethasone, 10 mmol/L β-sodium glycerol 3-phosphate, and 50 mg/L ascorbic acid.

2.6.2. Isolation and culture of cells

As mentioned earlier, BMSCs were purchased from Cyagen (China),

and the 4–6 passages were used for cell culture. For TDCs, after euthanasia of male Sprague-Dawley (SD) rats (100–120 g), the tendon tissue was harvested. After rinsing with sterile PBS, the tissue was cut into pieces and cultured in complete α-MEM, and then TDCs were obtained. The medium was changed every 3 days and the TDCs at 2–4 passages were used for subsequent studies [42].

2.6.3. Osteogenic differentiation of BMSCs and TDCs

The BMSCs and TDCs were seeded on cover glasses in 24 well plates at a density of 2×10^4 cells/well for immunofluorescence staining, and cells were seeded in 12 well plates at a density of 4×10^4 cells/well for other experiments. After 24 h' incubation, the cells grew to about 80 % confluence, and then the medium was replaced with OG medium. Three different groups including iCSP-Scr^P, iCSP-Scr^H and DP (100 × degradation product of iCSP-Scr^P) were set, and the cells treated with pure OG medium were set as control. Cell culture medium was changed every 3 days. After 7 and 14 days, the cells were fixed with 4 % paraformaldehyde and washed three times with sterile PBS, and alkaline phosphatase (ALP) staining was conducted using the BCIP/NBT Alkaline Phosphatase Color Development Kit (Beyotime, China) following the protocol provided by the manufacturer. The cells stained with ALP were observed and photographed using a mobile phone (Huawei P50, China) and an inverted fluorescent microscope (Olympus CKX41, Tokyo, Japan). The effect of iCSP-Scr to the expression of ALP by BMSCs and TDCs was also quantitatively assessed by Alkaline Phosphatase Assay Kit (Beyotime, China) on the 3rd, 7th and 14th day after initiation of osteogenic differentiation by the addition of OG medium.

The effect of iCSP-Scr to the expression of the related genes and proteins during the osteogenic differentiation of BMSCs and TDCs was also investigated via quantitative polymerase chain reaction (qPCR) and immunofluorescence staining. On the 7th day, the cells were harvested, the total cellular RNA was extracted by lysis in Trizol (TransGen Biotech, Beijing), which was then reverse-transcribed into cDNA with a cDNA Reverse Transcription Kit (TransGen, China). The qPCR was performed using PerfectStart® Fast Green qPCR SuperMix (TransGen, China) with QuantStudio 5 Real-Time PCR System (Thermo Fisher Scientific, USA). The PCR cycling consisted of 40 amplification cycles, with each cycle lasting for 5 s at 94 °C and 30 s at 60 °C. The relative level of expression of each target gene was calculated using the $2^{-\Delta\Delta Ct}$ method. All primers (Sangon Biotech, China) were summarized in Table S2. The gene expression levels of ALP, runt-related transcription factor 2 (Runx2), osteocalcin (OCN), and type I collagen (Col1) of BMSCs and TDCs, and the expression of scleraxis (SCX), tenomodulin (Tnmd), and tenascin-C (TnC) of TDCs, were calculated and normalized to the internal standard gene glyceraldehyde-3-phosphate dehydrogenase (GAPDH, Sangon Biotech, China), n = 3. And on the 7th day, the cells were fixed and immunofluorescence stained with OCN and Col1 following the procedures listed below: the fixed cells were blocked with QuickBlock™ Blocking Buffer (Beyotime, China) for 10 min, followed by incubation with Anti-Collagen I (P14695, Proteintech, USA) or Anti-OCN (P23418, Proteintech, USA) at 4 °C overnight, the cells were then incubated with second antibody conjugated with Dylight 488 (A23220, Abbkine, USA), and the nuclei were stained with DAPI (Beyotime, China). The Col1 and OCN immunofluorescence-stained cells were observed with LSCM, and the immunofluorescence intensity was analyzed using ZEN software, n = 5.

2.7. In vivo bone-tendon healing experiments

All *in vivo* animal experimental procedures were conducted in accordance with Arrive's guidelines and approved by the Institutional Animal Care and Use Committee (IACUC) of Nanfang Hospital (Permit No. IACUC-LAC-20221028-004), and performed according to the Animal Welfare Act and National Institute of Health (NIH) guidelines for the care and use of laboratory animals. New Zealand rabbits (male, 3 months old, 2.0–2.5 kg) were purchased from the Experimental Animal Center of Southern Medical University.

2.7.1. ACL reconstruction in rabbit models

The 24 New Zealand rabbits were randomly and evenly divided into two groups. The control group was treated with 3 mm diameter titanium screws (Natton, Beijing, China), while the iCSP-Scr group being treated with iCSP-Scr (CPU–$NCO_{0.5}$/PC-$HAp_{0.1}$ H_2O_{200}($P_{0.05}$)). Each group has two time points, 4 and 14 weeks (n = 6). To obtain sterile iCSP-Scr used for ACL reconstruction, the CPU-NCO was synthesized in a closed system to preserve sterilization status, and was then packaged under sterile conditions. Moreover, PC-HAp, porogen, and water were all sterilized by 5 kGy gamma ray irradiation [43].

Rabbits were anesthetized with pentobarbital sodium (30 mg/kg) by intravenous injection. The left leg was shaved and disinfected and an incision was created along the medial side of the rabbit's patella, and the patella was flipped outward to expose and remove the ACL. The semitendinosus was separated and harvested for subsequent ACL reconstruction. The rabbit knee joint was fixed at 45° flexion, and the bone tunnel which diagonally from the cortical bone on the inner side of the tibial joint surface towards the joint, exit at the ACL tibial attachment point, and then from the ACL femoral attachment point to the posterolateral side, was created using a 3 mm diameter drill. The bone tunnel was rinsed with physiological saline. Then the tendon substitute was pulled into the femoral tunnel at 30° in the knee flexion position, iCSP-Scr was injected and uniformly administrated into the gap between the tendon graft and the bone tunnel, and allowed to set and solidify (Fig. S7). For the control group, the tendon graft was fixed by a titanium screw (Φ3 mm) (Fig. S8). Meanwhile, to prevent the tendon graft from being pulled out before the iCSP-Scr fully solidified, the end of tendon graft for both groups was knotted and fixed to the tissue near the opening of the tibia and femur tunnel. Then the tissue was rinsed, sewed layer by layer, and disinfect with iodine. All rabbits were allowed free activity 2 h post-operation.

2.7.2. Micro-CT

At week 4 and 14 after surgery, the rabbits were euthanized via an overdose of anesthesia. The treated rabbit femur-tendon graft-tibia complex was harvested, the periosteum and surrounding soft tissue were removed, and only the femoral end sample was retained and fixed in 4% paraformaldehyde. The samples were scanned using Bruker Micro-CT Skyscan 1276 system to observe tendon-bone repair performance. Scan settings are as follows: voxel size 10 μm, medium resolution, 85 kV, 200 μA, 1 mm Al filter with the integration time of 384 ms.

Due to the presence of artifact in the CT results of titanium screws, it would affect the bone densities and related values, thereby affecting data analysis. Therefore, this study directly used Mimics Research 21.0 software to conduct three-dimensional reconstruction of micro-CT sectional images to analyze bone distribution inside and around bone tunnels. And to compare the new bone formation of iCSP-Scr groups at week 4 and 14, the bone mineral density (BMD) and bone volume/tissue volume (BV/TV) values were calculated using CTAn image analysis software.

2.7.3. Histological study of undecalcifed tissue sections

Due to the presence of titanium screws, hard tissue sections were performed to observe the boundary between the material and tissue. The fixed samples were dehydrated in gradient ethanol and xylene, soaked in methyl methacrylate containing dibutyl phthalate and benzoyl peroxide for 7 days to embed the tissue in poly(methyl methacrylate) (PMMA) block. The tissue blocks were sliced into 300 μm slices with a hard tissue microtome (Leica SP 1600, Wetzlar, Germany), then the slices were further ground to 80–100 μm with a grinder (RF-1, Ruifeng Instrument, China), and then the slices were polished to remove the grinding marks with talcum powder. The slices were soaked in 0.1% formic acid for 3 min and 20% methanol for 2 h, rinsed with PBS for 3 min before the performance of Van Gieson (VG) and Goldner Trichrome staining

according to the instructions. Then the stained slices were scanned with a Digital Easy Scan machine (Motic, China).

2.7.4. Biomechanical tests in vivo

After 14 weeks post-surgery, the biomechanical tests were performed on the femur-tendon graft-tibia complexes (Fig. S9). All soft tissues around the obtained femur-tendon graft-tibia complexes, and the knots of the tendon ends at the tunnel were removed before testing. The biomechanical properties of the reconstructed ACL were measured using an Instron 34TM-10 testing machine equipped with a 10 kN load cell. The tendon graft of the specimen was aligned parallel to the two vertical beams of the mechanical machine, and the load was applied with a load displacement rate at 0.5 mm/min. The maximum ultimate load until failure (N) was recorded, n = 3.

2.8. Statistical analysis

Data were presented as mean ± standard deviation (SD) of at least 3 independent experiments and analyzed with SPSS version 26. The Shapiro-Wilk test was used to evaluate the normal distribution of data. For data with normal distributed values, independent sample *t*-test was used for comparison between two groups, while one-way ANOVA was used after Bonferroni correction to analyze the differences between the multiple groups. For non-parametric data, Mann Whitey test was used for two groups, and Kruskal Wallis test was used for comparisons among multiple group comparisons. All data are considered to have statistical differences only when $p < 0.05$. *, **, and *** represent $p < 0.05$, $p < 0.01$ and $p < 0.001$, respectively.

3. Results and discussion

Currently, the most frequently used bone-tendon fixation mechanism in clinical ACL reconstruction is the compression mode using screws made of metal, biodegradable/non-degradable polymers and their composites with inorganic minerals, to compress tendon graft on one side of the bone tunnel wall in a punctiform ("point-to-point") manner. This fixation mode and the squeeze caused by screw threads generates shear force to the tendon graft and always induces stress concentration, making the tendon graft prone to fracture on the outer edge of the bone tunnel at the fixation point by the screw. Inspired by the rope-grasping mode in the tug-of-war sport where the rope is held in a planar ("surface-to-surface") manner by two or multiple hands, an innovative bone-tendon fixation paradigm was developed with the bone tunnels of femur and tibia simulating the hands of athletes, and tendon graft simulating the rope. The effective grip of the rope by the hands is the essential prerequisite for successful ACL reconstruction. To realize this, an injectable citrate-based bioactive self-expansive and planar-fixing screw (iCSP-Scr) was developed and evenly administrated into the bone-tendon gap. The instant expansion of iCSP-Scr in the confined space of the bone tunnel is expected can fulfill the bone-tendon gap even when some irregular shapes exist, and embed into and fuse with bone matrix, enables effective grip of the tendon graft and strong mechanical interlock between bone tunnel and iCSP-Scr, thus ensures strong bone-tendon fixation. The possible lateral swing of the tendon graft caused by the existence of bone-tendon gap could also be principally eliminated. Thereafter, along with the degradation of iCSP-Scr and the continuous release of osteogenic and bioactive ingredients from iCSP-Scr, such as citrate, PC and HAp, new bone growth would uniformly occur alongside the whole bone tunnel, further narrows down the bone tunnels and guarantees sustainable effective bone-tendon fixation and promotes bone-tendon healing *in vivo*.

3.1. Synthesis of CPU-NCO and PC-HAp

The synthesis routes of CPU-NCO and PC-HAp were shown in Figs. 1A and 2A. To confer CPU-NCO with bioactivity especially osteogenic activity, citrate, which possesses remarkable chemical and biological benefits in osteogenesis [25,31,34,44], was introduced. The introduction of citrate-based polyol as well as PCL triol ($M_n = 370$ Da) is also beneficial to increase the branching density of the obtained CPU-NCO thus the functionality density of the terminal –NCO groups. The successful synthesis of CPU-NCO was confirmed by the show up of the strong characteristic peak of –NCO at 2260 cm^{-1} in the FTIR spectrum of CPU-NCO (Fig. 2B). While, after crosslinking, the peak at 2260 cm^{-1} totally disappeared in the ATR-FTIR spectrum of crosslinked CPU (Fig. 2B). To endow HAp with possible chemical reactivity with CPU-NCO and enhance the organic/inorganic integration compatibility, PC, a typical plant-based polyphenol with multiple phenolic hydroxyl groups and two aliphatic hydroxyl groups, was used to chemically deposit on the surface of HAp at slightly basic condition (Figs. 1A and 2A). As shown in Fig. 2C, in the ATR-FTIR spectrum of PC-HAp, the characteristic groups derived from PC that making PC-HAp distinguish from HAp, namely the hydroxyl (-OH) group at ~ 3580 cm^{-1} and the benzene ring group at ~ 1610 cm^{-1} (especially the later one), appeared, indicating the successful introduction of PC on PC-HAp.

3.2. Preparation and optimization of iCSP-Scr

As shown in Fig. 1B, the injectable iCSP-Scr was prepared through mixing CPU-NCO/PC-HAp composite with water (with/without PEG-DM as porogen). The preserved –NCO groups in CPU-NCO reacted with water to generate carbon dioxide (CO_2), resulting in the expansion of material and pore formation; thus-obtained $–NH_2$ groups further reacted with the remaining –NCO groups to form crosslinked porous three-dimensional (3D) matrix, and the water-soluble PEG-DM could be washed out *in vivo* to form more pores. The –NCO groups can also react with the $–NH_2$ groups on tissue surface to enhance tissue adhesion. In principle, higher amount of water should generate more CO_2, resulting in higher expansion rate and porosity as well as lower Young's moduli and hardness of the crosslinked iCSP-Scrs. But the total amount of –NCO groups in CPU-NCO is limited, and the fluidity of the iCSP-Scr formulation would also affect the expansion and crosslinking process. Preliminary experiments indicated that the component ratios of between CPU-NCO, PC-HAp, and water (±porogen) can affect the expansion rate, hardness, and other mechanical properties of the obtained iCSP-Scrs. Therefore, to obtain iCSP-Scr with more satisfactory performance, the properties of the iCSP-Scrs with different formulations (CPU–NCO/PC-HAp H_2O(porogen)) were systematically studied by changing one variable and keeping the others unchanged each time (Table 1).

When the amounts of CPU-NCO, PC-HAp, and porogen were kept as 0.5 g, 0.1 g, and 0 g respectively (Table 1), as the water amount increased from 50, 100, 200–300 μL, and the expansion rate first increased and then decreased (Table 1 and Fig. 3A1). Among them, when the amount of water was 50 μL, the PC-HAp powder could not be evenly mixed with the liquid, while the mixture was too diluted to be applied when 300 μL water was used. And 100 and 200 μL water induced no statistical difference in the expansion rate. With changes in water amount, the trend of expansion rate and porosity (measured with the volumetric method) were the same (Fig. 3A2). In terms of Young's moduli and compression strengths, the group with 50 μL water was the highest, and there was no statistical difference among the other three groups (Fig. 3A3 and 3A4). After being crosslinked for 8 h, the hardness of the crosslinked CPU-$NCO_{0.5}$/PC-$HAp_{0.1}$ H_2O_x(porogen) gradually increased as the amount of water (x) increased gradually from 100, 200–300 μL, but no statistical difference was found in the hardness among all tested groups after 24 h (Fig. 3A5). Thus, the optimal amount of water was designed to be 200 μL when the amounts of CPU-NCO, PC-HAp, and porogen were roughly set as 0.5 g, 0.1 g, and 0 g respectively.

When the amounts of CPU-NCO, water, and porogen were kept at 0.5 g, 200 μL and 0 g respectively (Table 1), as the amounts of PC-HAp or HAp increased from 0, 0.1–0.2 g, the expansion rates and porosities of

both the obtained iCSP-Scr^{P} and iCSP-Scr^{H} decreased (Fig. 3B1 and 3B2), while the Young's moduli, compression strengths, and hardnesses all gradually increased (Fig. 3B3-3B5). When the amount of PC-HAp or HAp was kept at 0.1 g, there was no significant difference in the expansion rates, porosities, Young's moduli, and compression strengths between iCSP-Scr^{P}s and iCSP-Scr^{H}s, while the hardnesses of iCSP-Scr^{P} were higher than that of iCSP-Scr^{H} (Fig. 3B). This might be caused by the possible chemical reaction between the aliphatic hydroxyl groups on PC-HAp with the –NCO groups on CPU-NCO. Thus PC-HAp was used in the final formulation and the amount ratio between CPU-NCO and PC-HAp was set as 0.5 g/0.1 g to preserve appropriate expansion rate and mechanical properties.

When the amounts of CPU-NCO, PC-HAp and water were kept at 0.5 g, 0.1 g and 200 μL respectively (Table 1), as the amount of porogen increased, the expansion rate and porosity slightly increased (Fig. 3C1 and 3C2), while the Young's modulus, compression strength, and hardness all decreased (Fig. 3C3-3C5). Therefore, the porogen amount was set as 0.05 g.

In summary, CPU-NCO$_{0.5}$/PC-HAp$_{0.1}$ H_2O_{200}($P_{0.05}$) composed with 0.5 g CPU-NCO, 0.1 g PC-HAp and 200 μL water containing 0.05 g porogen, was determined possess the most balanced performance, and therefore chosen as the optimized iCSP-Scr formulation and used for the subsequent experiments.

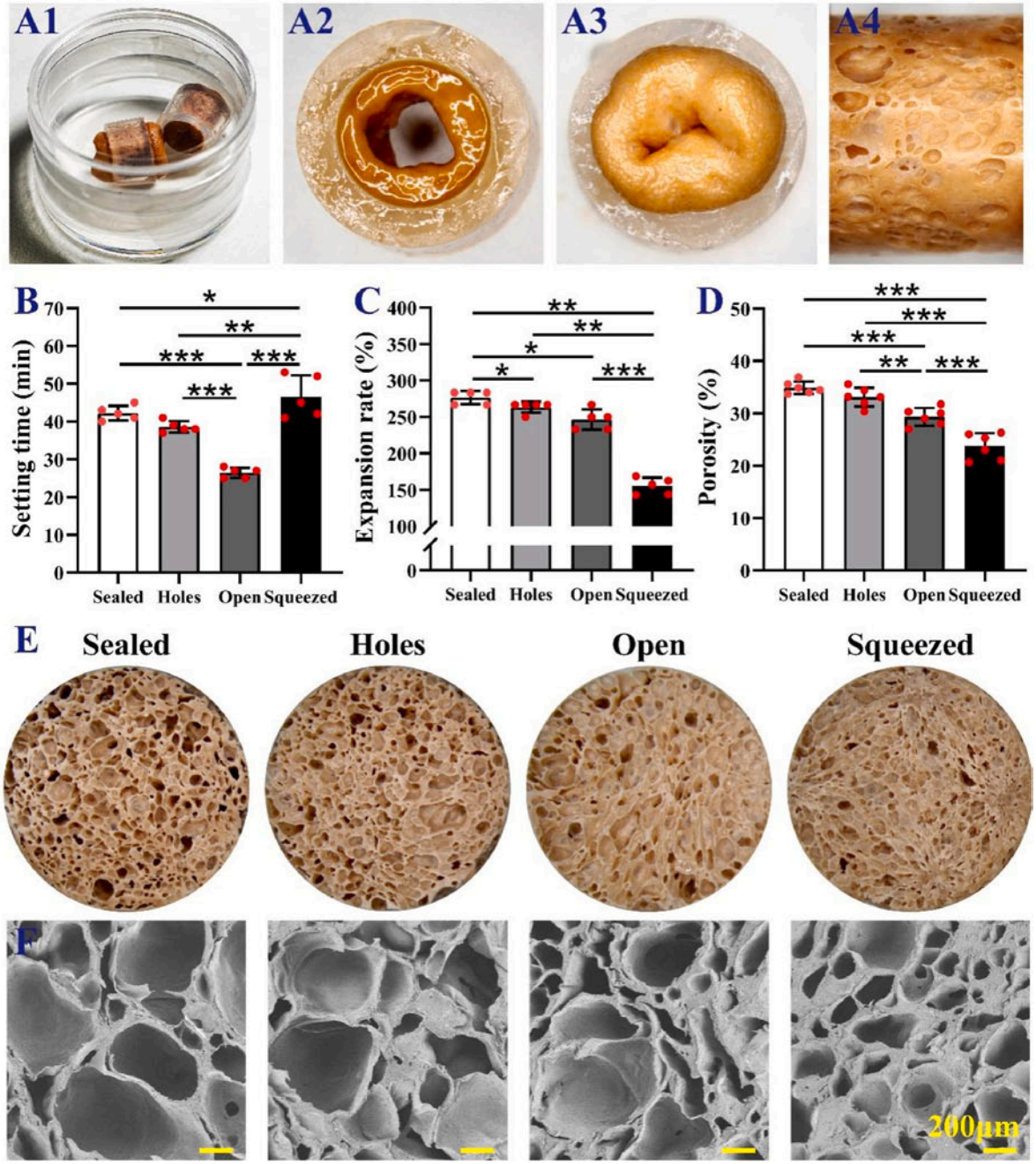

Fig. 4. The changes of iCSP-Scrs before and after expansion during *in vitro* simulated ACL reconstruction (A1-A4). The setting time (B), expansion rate (C), porosity (D), and morphology under stereoscopy (E) and SEM (F) of iCSP-Scrs in different sealing conditions. n = 5. *, **, and *** represent $p < 0.05$, $p < 0.01$ and $p < 0.001$, respectively.

3.3. Characterizations of iCSP-Scr crosslinked in confined space

The injectability of iCSP-Scr was demonstrated through the process of writing "SMU" using iCSP-Scr (Fig. S1 and Video S1), and the injection force from a 5 mL syringe (without the needle) was also measured to be 4.0 ± 0.53 N (Fig. S2B). Since the pores of iCSP-Scr were created by the generated CO_2 during crosslinking, the relatively weak expansive force of gas destined that the expansion of iCSP-Scr would be greatly limited in confined space, and the expansion of iCSP Scr was influenced by the size and airtightness of the space. During ACL reconstruction, the iCSP-Scr was injected into the gap between tendon and bone tunnel in the knee joint cavity, an incompletely sealed confined space. To simulate ACL reconstruction *in vitro*, the bone tunnel was simulated using transparent silicone tubes with iCSP-Scr being evenly smeared into the inner side of the tube wall, and allowed to crosslink in a sealed dish (Fig. 4A1 and 4A2). As shown in Fig. 4A3, the expanded iCSP-Scr nearly filled all the tube, graphically suggesting that in the actual situation when iCSP-Scr was administrated in bone-tendon healing, the tendon graft would be strongly squeezed and fixed in the bone tunnel by the injected iCSP-Scr. And numerous pores with variable sizes can be seen on the surface of the expanded iCSP-Scr (Fig. 4A4).

To comprehensively investigate the properties of crosslinked iCSP-Scrs in incompletely sealed confined space stimulating the situation of ACL reconstruction, iCSP-Scrs (with the optimized formulation CPU-$NCO_{0.5}$/PC-$HAp_{0.1}$ H_2O_{200}($P_{0.05}$)) were crosslinked in 2 mL tubes, under two extreme states, namely completely sealed (Sealed) and completely unsealed (Open), and two intermediate states including incompletely sealed (Holes, simulates ACL reconstruction) and incompletely sealed plus external forces (Squeezed) (Fig. 2A and Table S2). From Fig. 4B, it can be seen that the setting times of the Sealed (42.20 ± 1.92 min) and Holes (38.60 ± 1.52 min) groups were all significantly longer than that of the Open (26.40 ± 1.34 min) group ($p < 0.01$). This might be caused by that the moisture in air increased the content of water thus speeded up the crosslinking process. While, the Squeezed group showed the longest setting time (46.00 ± 5.96 min) in all the tested groups, since higher solid content would generate more CO_2 thus take longer time to set and stop expansion (Fig. 4B). In terms of expansion rate, the value of the Holes group was 263.33 ± 7.45%, which had no significant

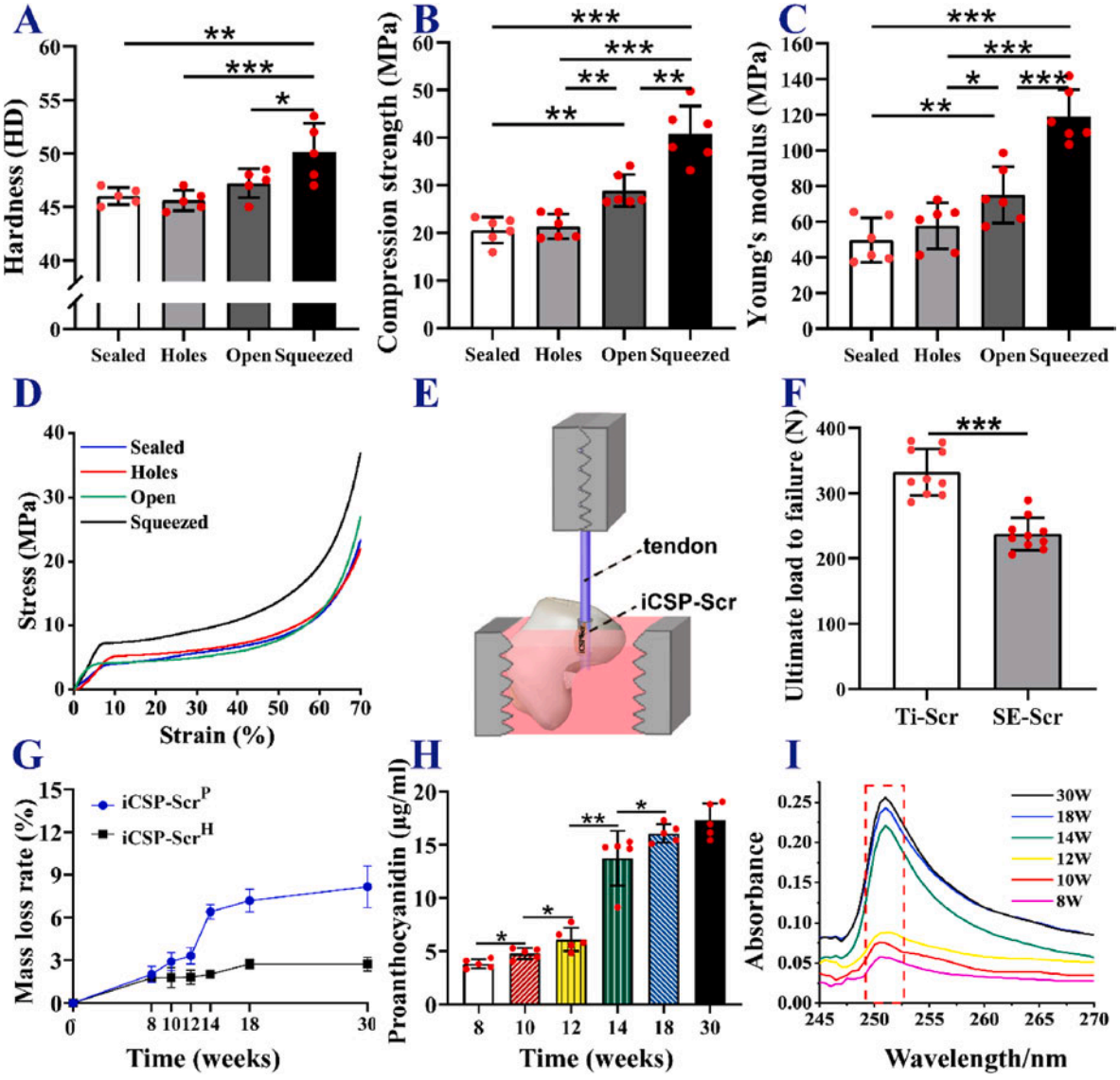

Fig. 5. The hardness (A, n = 5), compression strength (B, n = 6), Young's modulus (C, n = 6), and strain-stress curve (D, n = 6) of iCSP-Scrs in different sealing conditions. The schematic diagram (E) and results (F) of pull-out performance testing (n = 10). Specifically, the bones were placed in the well mixed mixture of pink denture base materials and prepared into a regular shape that was easy to grip (E). The degradability (G), and proanthocyanidins release (H and I) of iCSP-Scr (n = 5). *, **, and *** represent $p < 0.05$, $p < 0.01$ and $p < 0.001$, respectively.

statistical difference compared to the Open group (246.67 ± 13.94%), but lower than that of the Sealed group (276.67 ± 9.13%) (Fig. 4C). Due to the administration of external force, the expansion rate of the Squeezed group was the lowest in all the four groups (155.00 ± 11.44%), significantly lower than the other groups (Fig. 4C). The porosities of the crosslinked iCSP-Scrs should be positively correlated with the expansion rate. As expected, the porosities of iCSP-Scrs gradually decreased from the Sealed, Holes, Open to Squeezed groups. The porosity of the Sealed group was higher than that of the Open group, which might be caused by the more CO_2 escaping when the lid opening compared to the sealed conditions, making it impossible to create pores inside the material. And the porosity of the Squeezed group was 23.72 ± 2.52%, significantly lower than that of the other groups (Fig. 4D). The same trend can be also reflected from the stereoscopy and SEM images, in which the Squeezed group also showed the shallowest pores than others, and the deepness and density of the pores of iCSP-Scrs gradually increased from Squeezed, Open, Holes to Sealed (Fig. 4E and F).

Based on the rheological results shown in Fig. S5, a cross point of storage modulus (G′) and loss modulus (G″) were observed at ~ 13 min (780 s), close to the setting time results shown in Fig. 4B, which represented the critical transition of iCSP-Scr from liquid to solid.

The hardness of the crosslinked iCSP-Scr is also close related to the porosity of iCSP-Scr. The overall hardnesses of all the iCSP-Scr samples crosslinked in 2 mL tubes were in the range of 45.60–50.10 HD (all >90 HA), significantly higher than that of the iCSP-Scrs crosslinked in 5 mL syringes, in which their hardnesses were 86.60 ± 2.30 HA. The Squeezed group exhibited the highest hardness (50.10 ± 2.70 HD), significantly higher than that of the other groups, while there was no statistical difference among the other three groups (all around 46 HD) (Fig. 5A). Along with decrease of porosity, the compression strengths of crosslinked iCSP-Scrs also gradually increased from 20.58 ± 2.72 MPa of the Sealed group and 21.36 ± 2.60 MPa of the Holes group, to 28.90 ± 3.33 MPa of the Open group, to 40.78 ± 5.90 MPa of the Squeezed group (Fig. 5B). And the Young's moduli exhibited a similar trend to the compression strengths, which gradually increased from 49.79 ± 12.46 MPa for the Sealed group, to 57.81 ± 12.88 MPa for the Holes group, 75.12 ± 15.88 MPa for the Open group and 118.99 ± 15.07 MPa for the Squeezed group (Fig. 5C). The effect of tube sealing condition to the mechanical strength could also be reflected by the representative stress-strain curves (Fig. 5D). These results roughly reflect the possible upper and lower limits of different indices for iCSP-Scrs crosslinked at different incompletely sealed conditions stimulating the actual situation of ACL reconstruction, and preliminarily reveal the relationships between the expansion rate, porosity, hardness, and compression performance.

As shown in the photographs of lap-shear test against wet porcine skin (Fig. S6), iCSP-Scr exhibited favorable tissue adhesion ability. Reactive polyurethane has been clinically utilized as tissue adhesive, such as TissuGlu approved by U. S. FDA for postoperative adhesion following abdominal liposuction.

To further evaluate the feasibility of iCSP-Scr in term of fixing tendon graft in bone tunnel, the pull-out resistance of tendon substitute (using woven nylon rope) from the bone tunnels created on pig's knee joints, was investigated (Fig. 5E). As shown in Fig. 5F, the ultimate load (until failure) of the iCSP-Scr group was 237.56 ± 24.94 N, significantly lower than that of the Ti screw group (332.44 ± 35.79 N). And it is worth to mention that, the failure of the Ti screw group almost caused by the breakage of the tendon substitutes at the outer edge of the bone tunnel fixed by the Ti screw, while the reason for the failure of the iCSP-Scr group was the pull out of tendon substitutes from the bone tunnels. The above results not only prove that Ti screws, as a traditional metal interference screw, can provide strong fixation in the early stages of ACL reconstruction, but also reflect that the application of traditional interference screw always causes stress concentration and excess squeeze to the tendon graft on where the screw was applied. While, for iCSP-Scr, the tendon graft was evenly squeezed if iCSP-Scr was evenly applied, and if proper amount of iCSP-Scr was applied to provide sufficient squeezing force, effective planar-fixing of tendon graft in bone tunnel could be achieved.

Moreover, the degradation profiles of iCSP-Scr^P and iCSP-Scr^H were assessed by the degradation study in PBS at 37 °C. As shown in Fig. 5G, although both iCSP-Scr^P and iCSP-Scr^H showed slow degradation, especially in the beginning 12 weeks, the degradation of iCSP-Scr^P became significantly faster than that of iCSP-Scr^H after 12 weeks. The mass loss of iCSP-Scr^P rapidly increased from 3.31 ± 0.57% at the 12th week to 8.15 ± 1.47% at the 30th week. While, the mass loss of iCSP-Scr^H was only 2.74 ± 0.49 % at the 30th week (Fig. 5G). The relatively faster degradation of iCSP-Scr^P comparing to iCSP-Scr^H might be attributed to the introduction of PC on the surface of HAp. The residual aliphatic or phenolic hydroxyl groups (especially the former one) of PC coated on HAp might be involved in the urethane-urea reaction during the crosslinking of iCSP-Scr^P, thus the detach of PC from PC-HAp would cause the disintegration of the crosslinked iCSP-Scr^P. On the other hand, comparing to ordinary urethane bond formed by –NCO and aliphatic hydroxyl group, the thermally reversible phenol-carbamate bond formed by the reaction between –NCO and phenolic hydroxyl group is easier to be hydrolyzed [39,40], also leading faster degradation of iCSP-Scr^P than that of iCSP-Scr^H. The release of PC from iCSP-Scr^P during degradation was also studied by detecting concentration of PC in the degradation solution via UV–vis spectrometer. It can be seen from Fig. 5H as time prolonged, the concentration of PC in the degradation solution gradually increased, consistent with the trend of degradation. The accumulative concentration of PC rapidly increased from 6.11 ± 1.11 μg/mL at the 12th week to 13.74 ± 2.58 μg/mL at the 14th week, and the final accumulative concentration of PC at the 30th week was ~17.28 ± 1.61 μg/mL. This can also be confirmed from the increase of the UV–vis absorbance of PC at ~250 nm in the degradation solution along with the increase of degradation time (Fig. 5I). These results preliminarily proved the biodegradability of iCSP-Scrs, especially iCSP-Scr^P, and iCSP-Scr^P is also able to release anti-oxidant PC, beneficial to improve the biocompatibility and enhance the bioactivity of iCSP-Scr^P comparing to iCSP-Scr^H.

3.4. Biocompatibility of iCSP-Scr in vitro

As shown in Fig. 6A and B, the cell viabilities of the degradation products of iCSP-Scr with different dilutions, including 1 × , were all close to or even higher than 100 % during the whole tested period from 1 day to 5 days, exhibiting no cytotoxicity against both BMSCs and TDCs. And for some dilutions, the degradation product was found can even promote cell proliferation, especially on day 3 and 5. For Live/Dead staining, BMSCs was co-cultured with iCSP-Scr^P, iCSP-Scr^H and 100 × degradation product of iCSP-Scr^P (DP) for 24 and 48 h. It can be seen from Fig. 6C and D that, almost no dead cells were found for all samples, and the numbers of living cells of iCSP-Scr^P and DP samples were higher than that of the control and iCSP-Scr^H groups after 24 and 48 h, indicating the favorable cell proliferation enhancing ability of iCSP-Scr, especially when PC was introduced on to HAp (iCSP-Scr^P). The cell scratch assay results were shown in Fig. 6E and F, it can be seen that the migration rate of iCSP-Scr^H group was significantly higher ($p < 0.01$) than that of the control group, and the inclusion of PC further improved the migration rates of iCSP-Scr^P and DP groups, with the migration rate of the DP group the highest. The favorable cell migration promoting ability of iCSP-Scr^P was believed derived from the inclusion of cell metabolism promoting citrate [34,45] as well as antioxidant PC [38]. The cell adhesion of BMSCs directly on porous iCSP-Scr^H after being cultured for 24 h was also observed. It was found that bare iCSP-Scr without cells could also stained blue by DAPI, thus under LSCM the cell nuclei could not be distinguished from the material, but the cell matrix was stained green with Calcein AM and made the cells visible (Fig. 6G). The BMSCs were found can adhere well on the pores of iCSP-Scr and exhibited stretched morphology. The SEM image also show that the cells extended filamentous and plate-like pseudopodia,

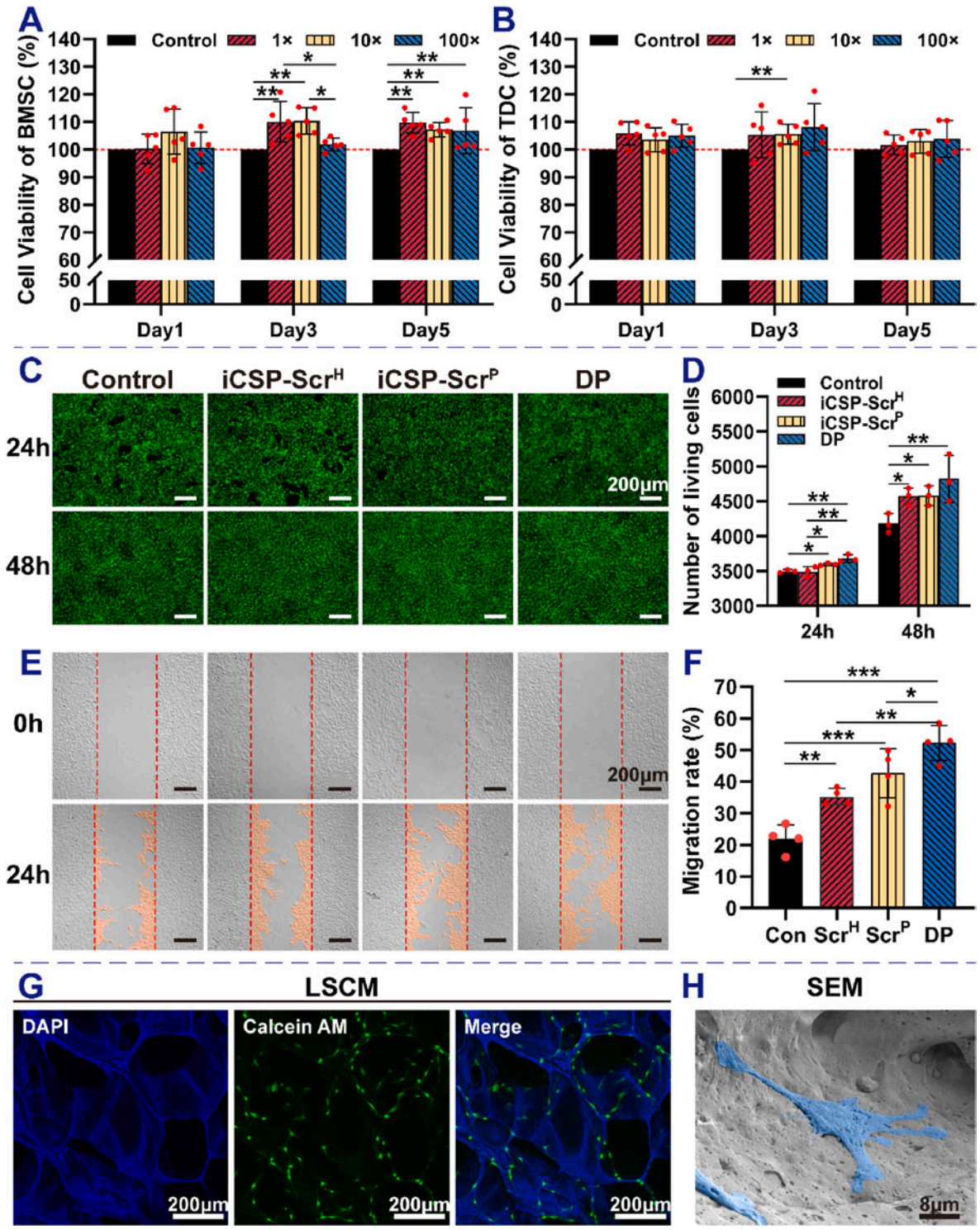

Fig. 6. The biocompatibility of iCSP-Scr in *vitro*. The cell viabilities of BMSC (A) and TDC (B), live/dead staining (C) and its number of living cells (D) of BMSC, qualitative (E) and quantitative (F) results of cell scratch experiments, and cell adhesion under LSCM (G) and SEM (H). Con, Scr^H, Scr^P, DP represents the control group, iCSP-Scr^H (CPU–$NCO_{0.5}$/$HAp_{0.1}H_2O_{200}$($P_{0.05}$)), iCSP-Scr^P (CPU–$NCO_{0.5}$/PC-$HAp_{0.1}H_2O_{200}$($P_{0.05}$)), and the degradation products group, respectively. *, **, and *** represent $p < 0.05$, $p < 0.01$ and $p < 0.001$, respectively.

spreading out in the pores of crosslinked iCSP-Scr (Fig. 6H).

The above results demonstrated that iCSP-Scr possesses favorable cytocompatibility, is able to promote cell adhesion, proliferation, and migration, well supporting the practical application of iCSP-Scr in bone-tendon healing.

3.5. *In vitro osteogenic properties of iCSP-Scr*

To systematically assess the osteogenic properties of iCSP-Scr *in vitro*, the effect of iCSP-Scrs to the ALP activity, the expression of osteogenic related genes including ALP, OCN, Runx2 and Col1 of both BMSCs and TDCs, the expression of tendon related genes (SCX, TnC and Tnmd) of TDCs, and the production of osteogenic proteins (OCN and Col1) by

BMSCs and TDCs was further investigated via ALP staining, quantitative ALP assay kit, qPCR, and immunofluorescence staining respectively.

As a key enzyme in the formation and metabolism of bone, ALP was an important indicator of osteogenesis [46]. From Fig. 7A and B, it can be seen that the inclusion of crosslinked iCSP-Scr^{H} and iCSP-Scr^{P} as well as the 100 × degradation product of iCSP-Scr^{P} (DP) in the osteogenic medium all increased the expression levels of ALP, and the ALP expression improvement for different samples were in the sequence of DP > iCSP-Scr^{P} > iCSP-Scr^{H}. Moreover, the ALP expression content increased with time from day 3, 7 to 14, and the ALP expression contents of the TDCs groups were lower than that of the BMSCs groups (Fig. 7A and B). These results preliminarily confirmed the osteoinductivity of iCSP-Scrs, especially when PC was included.

Furthermore, the effect of iCSP-Scr to the osteogenic related genes, including ALP, Runx2, OCN, and Col1, was assessed using both BMSCs and TDCs as the cell models. Among these genes, Runx2 was considered as an early indicator and the central gene involved in the osteoblast phenotype induction [47], while OCN was a marker of osteoblast maturation [38]. Col1 accounted for 90 % of the total organic components of bone matrix, thus was crucial for the embryonic development of the skeletal system, as well as the maintenance and repair of bones [48]. It can be seen that after being treated with osteogenic differentiation medium for 7 days, the inclusion of iCSP-Scr^{P}, iCSP-Scr^{H} and DP all led to higher gene expression levels of ALP, Runx2, OCN, and Col1, than that of the control group, by either BMSCs or TDCs (Fig. 7C–J).

SCX was the marker of both precursor and mature tendon cells [49],

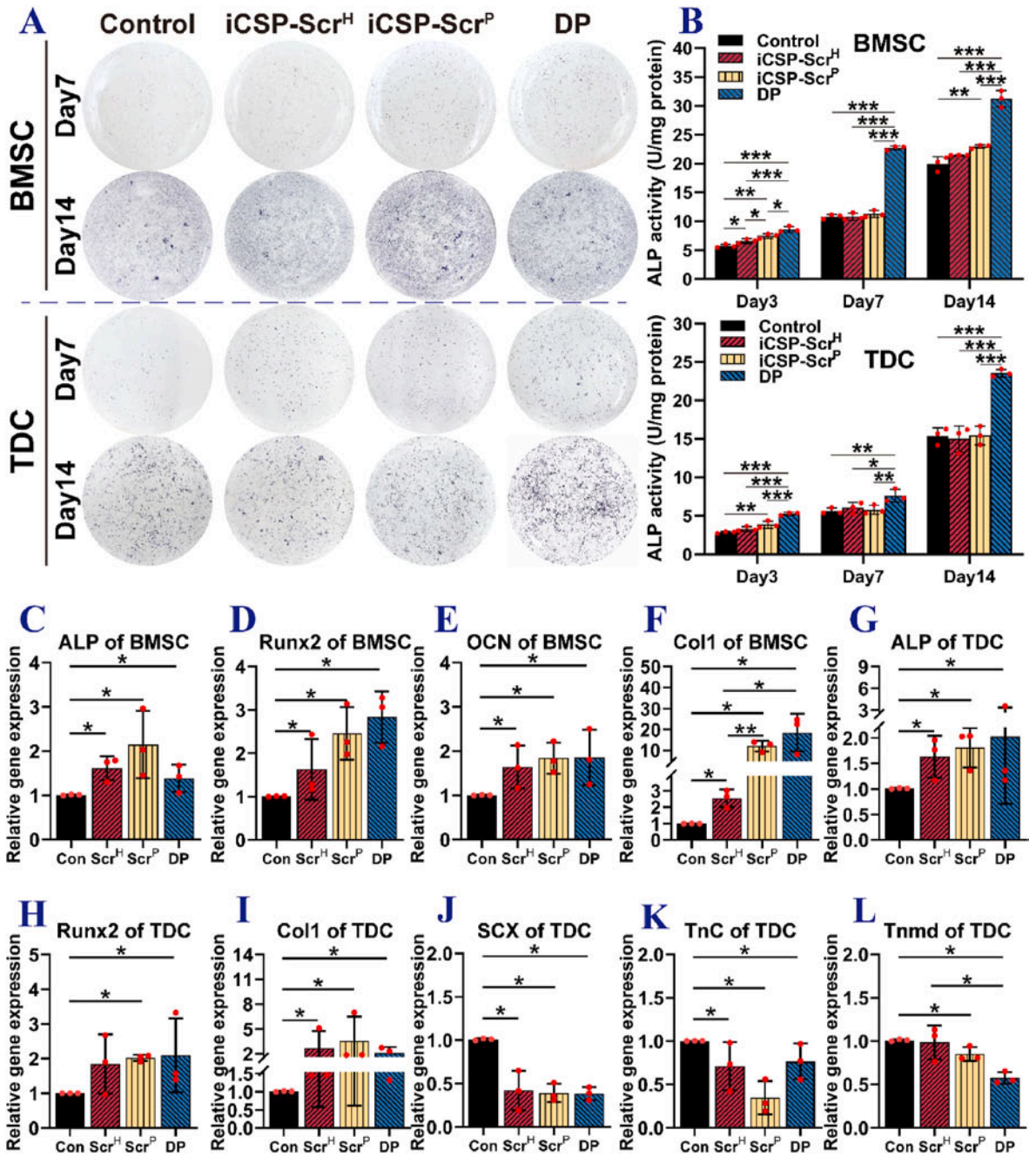

Fig. 7. The results of ALP staining (A), alkaline phosphatase assay kit results(B), and PCR results of BMSC and TDC (C–M). Con, Scr^{H}, Scr^{P}, DP represents the control group, iCSP-Scr^{H} (CPU–$NCO_{0.5}$/$HAp_{0.1}H_2O_{200}$($P_{0.05}$)), iCSP-Scr^{P} (CPU–$NCO_{0.5}$/PC-$HAp_{0.1}H_2O_{200}$($P_{0.05}$)), and the degradation products group, respectively. n = 3. *, **, and *** represent $p < 0.05$, $p < 0.01$ and $p < 0.001$, respectively.

TnC extensively existed around collagen fibers and the tendon cells [50], and Tnmd was the well-recognized marker gene of mature tendons [51]. As shown in Fig. 7K–L, after being treated with osteogenic medium for 7 days, the iCSP-Scr^{P}, iCSP-Scr^{H} and DP groups all showed the down regulation of the expression levels of SCX, TnC and Tnmd comparing to that of the control group. The above qPCR results showed that iCSP-Scr and its degradation products not only promoted the expression of bone related genes in both BMSCs and TDCs, but also suppressed the expression of tendon related genes in TDCs (Fig. 7). This might be caused by the presence of tendon stem cells with multidirectional differentiation potential in the tendon tissue [52], thus-obtained TDCs underwent a transition from tendinous differentiation to osteogenic differentiation in the osteogenic induction conditions. The iCSP-Scr and its degradation product were proved possess superior osteoinductivity than the control group, also implying that the application of iCSP-Scr has the potential to promote bone-tendon integration during ACL reconstruction.

Finally, to visually evaluate the effect of iCSP-Scrs to the osteogenic differentiation and collagen production of BMSCs and TDCs, Col1 and OCN immunofluorescence staining was conducted. As shown in Fig. 8A and B, for the OCN protein expression of BMSCs after 7 days' treatment, the levels of the iCSP-Scr^{H} and iCSP-Scr^{P} groups were nearly the same as that of the control group, but the DP group showed significantly improved OCN expression level comparing to the control, iCSP-Scr^{H} and iCSP-Scr^{P} groups. This might be caused by the low concentration of released active constituents by iCSP-Scr^{H} and iCSP-Scr^{P} scaffolds comparing to the DP sample. While, when treated TDCs, the iCSP-Scr^{H} and iCSP-Scr^{P} groups induced improvement of OCN protein expression (Fig. 8E and F). The iCSP-Scr^{H}, iCSP-Scr^{P} and DP groups all promoted the protein expression of COl1 of both BMSCs and TDCs, with the protein expression levels of the iCSP-Scr^{P} and DP groups higher than that of the

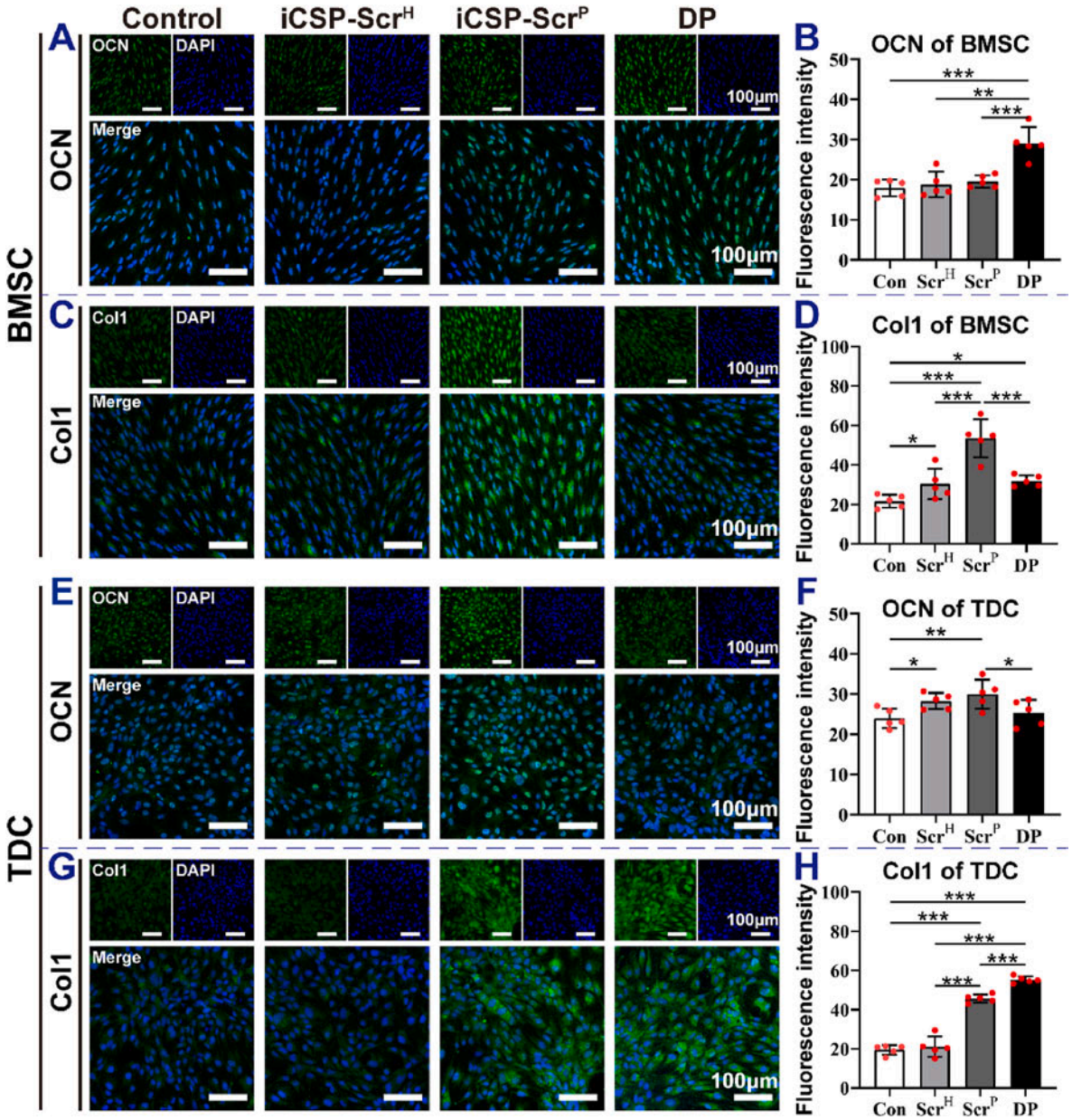

Fig. 8. Immunofluorescence results and statistical analysis of their immunofluorescence intensity. In the immunofluorescence results taken with LSCM, such as the control group in A, the image on the top left is the target protein stained with green fluorescence, the image on the top right is the cell nucleus stained with DAPI, the image below is the merge result of the two images above, and their scale bars are 100 μm. Con represents the control group, Scr^{H} represents iCSP-Scr^{H} (CPU–$NCO_{0.5}$/$HAp_{0.1}H_2O_{200}$($P_{0.05}$)), Scr^{P} represents iCSP-Scr^{P} (CPU–$NCO_{0.5}$/PC-$HAp_{0.1}H_2O_{200}$($P_{0.05}$)), and DP represents the degradation products group. n = 3. *, **, and *** represent $p < 0.05$, $p < 0.01$ and $p < 0.001$, respectively.

iCSP-Scr^{H} group (for TDCs, $p < 0.001$) (Fig. 8C, D, 8G and 8H). These results further proved the favorable osteoinductivity of iCSP-Scrs in the protein level.

All the above results showed that the presence of iCSP-Scr, especially iCSP-Scr^{P}, in the osteogenic medium can promote both the osteogenic differentiation and extracellular matrix synthesis of BMSCs. Moreover, the presence of iCSP-Scr could also promote the osteogenic differentiation of TDCs while suppress the expression of tendon related genes in TDCs, also preliminarily proving that implanted tendon grafts have the potential to be transformed into bone at the cellular level.

3.6. ACL reconstruction in rabbits

To further prove the concept of self-expansive polyurethane-urea as injectable screw and verify the *in vivo* tendon graft fixation and bone-tendon healing efficacy of iCSP-Scrs, the ACL reconstruction effect with the sterile representative iCSP-Scr (CPU–$NCO_{0.5}$/PC-$HAp_{0.1}$ H_2O_{200}($P_{0.05}$)) was investigated in rabbit models, using commercially available Ti screw as control. Micro-CT analysis, and histological staining on hard tissue slices, as well as biomechanical studies were conducted at 4 and 14 weeks postoperatively.

It was well known that artifacts always exist in the Micro-CT results of metal screws [53]. Thus, although the 3D reconstructed Micro-CT images (point by red arrows in Fig. 9A and C) and the 2D Micro-CT images (point by red arrows in Fig. 9B and D) of the Ti screw group at 4 and 14 weeks exhibited a decrease of internal cavity, it cannot evidence any bone ingrowth inside the Ti screws. This was further proved by the VG and Goldner Trichrome staining results of the Ti screw group at 4 and 14 weeks (point by red arrows in Fig. 9I and O). While, for the iCSP-Scr group, at 4 weeks after surgery, there were granular bone like particles (visible by Micro-CT) dispersed along the whole bone tunnel (colored particles in Fig. 9E and F), and bone like clumps could also be seen at the outer edge of the bone tunnel (point by green arrows in Fig. 9E and F). There was a significant increase of bone like particles in the bone tunnel at 14 weeks (colored particles in Fig. 9G and H). The favorable and uniform osteogenesis in the whole bone tunnel was beneficial for the recovery of the physiological structure of tendon-bone, thereby improving the bone-tendon fixation strength in a biological way and avoiding possible stress concentration. For the Ti screw group, quantitative analysis was meaningless due to the presence of artifacts in the CT results. Therefore, only the CT results of the iCSP-Scr group were quantitatively analyzed. The increase in BMD (Fig. 9Q) and BV/TV (Fig. 9R) of iCSP-Scr group over time from week 4 to week 14 demonstrated the osteogenesis-promoting effect of iCSP-Scr in *vivo*.

As shown in the VG and Goldner Trichrome staining results, no new bone formation could be found in the hollow interior of Ti screws at either 4 or 14 weeks after surgery (point by red arrows in Fig. 9I and O). This further proving that the false impression of the Ti screws being filled with bone reflected by the 3D micro-CT images (Fig. 9A and C) was caused by the artifacts of Ti screws, confirming that Ti screws were unable to promote bone ingrowth. For the iCSP-Scr group at week 4, it can be seen that the injected iCSP-Scr expanded and completely fulfilled the irregularly shaped bone tunnel and formed favorable mechanical interlock between bone tunnel and iCSP-Scr (as pointed by dark blue arrows in Fig. 9J, L, and 9 N). New bone formation was observed at the interface between iCSP-Scr and tendons, as well as at the interface between iCSP-Scr and bones (green arrows in Fig. S10E). And at 14 weeks, cracks and bone like substances appeared inside the crosslinked and expanded iCSP-Scr (Fig. 9P and locally enlarged in Fig. S10H), further confirming the new bone growth phenomenon reflected by the 3D Micro-CT images (Fig. 9E and G). Moreover, at week 14, at the interfaces between iCSP-Scr and tendons/bones, new bone formation was significantly higher than that of week 4 (green arrows in Figs. S10G and S10H). In addition, the VG and Goldner Trichrome staining results also show that due to the close or even identical inner diameters of the bone tunnel and Ti screw, the tendon graft was strongly compressed and severely deformed by the thread compression of the Ti screw (light blue arrows in Fig. 9I, M, and S10A-D). While, in the iCSP-Scr group the tendon grafts were flattened by the expanded iCSP-Scr located in the bone tunnel, resulting in more compact bone-tendon fixation (light blue arrow in Fig. 9P, and S10E-H). These would be further enhanced by new bone ingrowth induced by the degradation of iCSP-Scr that not only vacates space but also provide osteogenic and bioactive constituents including citrate, PC and HAp.

The *in vivo* biomechanical study results (Fig. 9S) showed that after 14 weeks of treatment, the pullout force (ultimate load) of the tendon graft from the bone tunnel for the iCSP-Scr group reached 106.2 ± 23.15 N, even slightly higher than that of the Ti screw group (93.8 ± 17.89 N). There was no statistical difference between these two groups because relatively few experimental animals. However, trustworthy conclusion can still be summarized based on the causes of tendon rupture. The Ti screw group still failed due to the rupture of the tendon fixed by the screw at the outer edge of the bone tunnel, while the reason for the failure of iCSP-Scr was no longer the tendon being pulled out, but the tendon being torn off. Retrospecting the *in vitro* biomechanical study results shown in Fig. 5F, it can be concluded that: although iCSP-Scr could not provide super strong tendon fixation comparable with that of metal screws merely relying on the squeezing force by the expanded iCSP-Scr in the bone tunnel (a typical confined space) and the mechanical interlock between bone tunnel and iCSP-Scr; while, with the enhancement of the osteogenic effect of iCSP-Scr derived from citrate, PC and HAp, iCSP-Scr can promote new bone inward growth of bone tunnel and enhance the bone/iCSP-Scr mechanical interlock, thus can provide effective tendon graft fixation and promote bone-tendon healing in ACL reconstruction *in vivo* (Fig. 9Q–S).

The biomechanical strength of iCSP-Scr after rabbit ACL reconstruction was even slightly higher than that of the Ti screw group. However, assuming that iCSP-Scr is applied to human ACL reconstruction, its mechanical performance remains unknown and full of challenging. In clinical practice, metal screws with a common diameter of 8 mm are typically used, and the human ACL ligament is significantly larger than the rabbit ligament. Additionally, the results of in *vitro* mechanical tests have shown that the pull-out strength of iCSP-Scr was lower than that of the 8 mm Ti screw group. Furthermore, the further impact of in *vivo* biology on the fixation of tendons with iCSP-Scr is unknown before conducting clinical experiments. Although the road ahead is full of challenges, there is hope that through continuous improvement, iCSP-Scr can achieve sufficient mechanical performance comparable to existing screws in clinical applications.

4. Conclusion

Traditional bone-tendon fixation strategies always limited by insufficient bone-tendon fixation, stress concentration, modulus mismatch between tissues and implants, and the possible lateral swing and longitudinal elongation of tendon. To address the aforementioned limitations, ingeniously utilized the incompletely sealed confined space of the bone-tendon gap and the moisture-induced crosslinking and expansion of polyurethane-urea, a kind of tug-of-war-inspired injectable citrate-based self-expansive and planar-fixing screw (iCSP-Scr) was developed for ACL reconstruction. The iCSP-Scr was composed with reactive isocyanate (NCO) terminalized citrate-based polyurethane (CPU–NCO) and proanthocyanidin (PC) modified HAp (PC-HAp), which was further mixed with water (with/without PEG-DM as a porogen) and administrated into the bone-tendon gap, to initiate the polyurethane-urea crosslinking and expansion process and realize effectively strong and stable bone-tendon fixation comparable with that of metallic screw through mechanical interlocking, physical expansion and chemical bonding. Furthermore, the developed iCSP-Scr was proved to possess favorable biocompatibility and biodegradability to release osteogenic constituents including citrate, PC and HAp, was able to promote the osteogenesis of BMSCs and TDCs, and also suppress the tendon

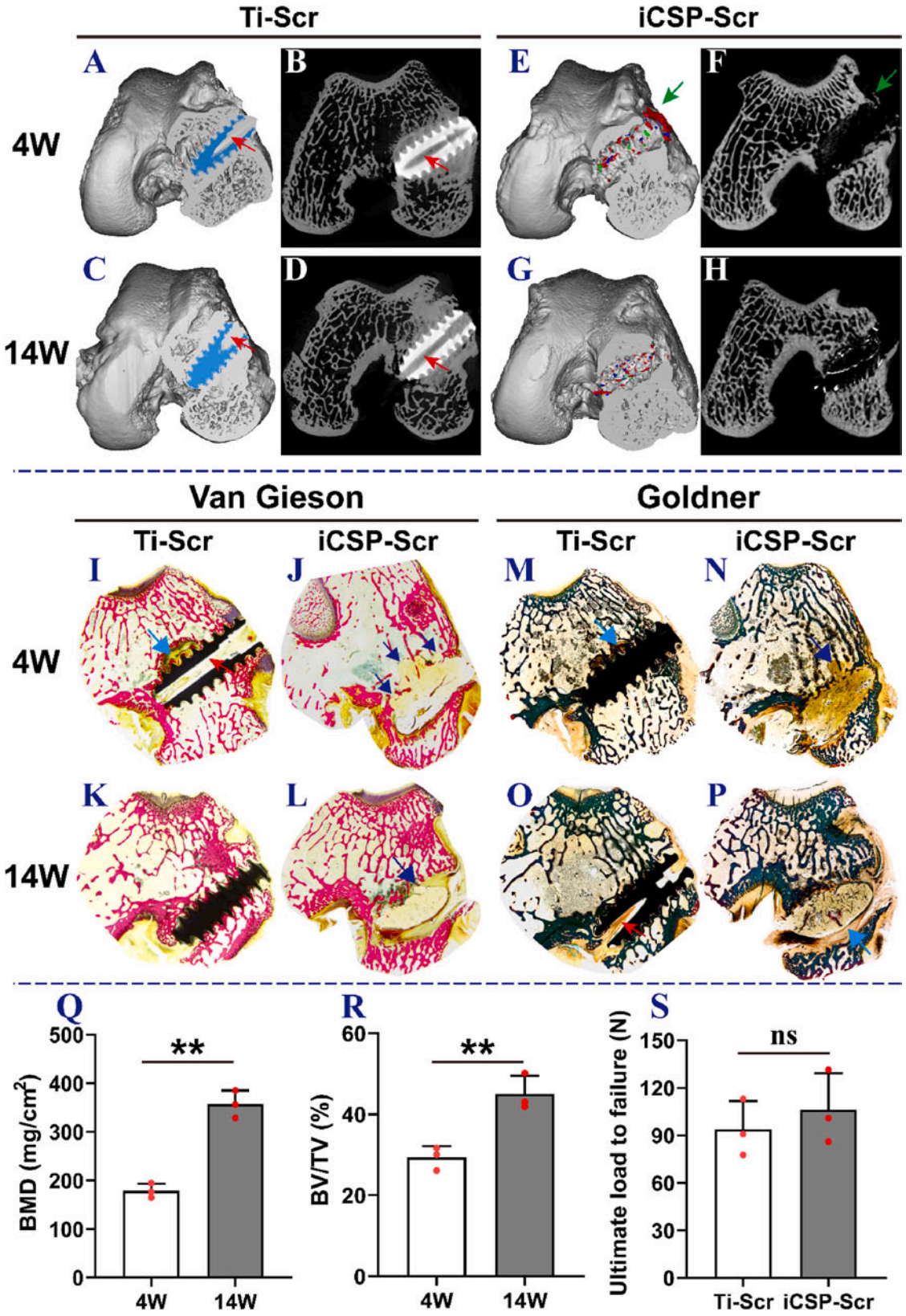

Fig. 9. ACL reconstruction in rabbits. The 3D reconstructed Micro-CT images and the 2D Micro-CT images (A–H), VG staining results (I–L), Goldner trichrome staining results (M − P), schematic diagram of ACL reconstruction in rabbits, the results of bone mineral density (BMD) (Q) and bone volume/tissue volume (BV/TV) (R) in iCSP-Scr group at 4W and 14W, and pull-out resistance performance *in vivo* (S). The red arrow represents the growth of bone in the hollow area inside the screw. The green arrow represents the bone like clumps at the outer edge of the bone tunnel. The light blue arrow represents the tendon, while the dark blue arrow represents the expansion and complete filling of crosslinked iCSP-Scrs in irregularly shaped bone tunnels. n = 3. *, **, and *** represent $p < 0.05$, $p < 0.01$ and $p < 0.001$, respectively. In addition, ns represents $p \geq 0.05$, indicating no significant statistical difference.

differentiation of TDCs in osteogenic microenvironment. The favorable osteoinductive ability of iCSP-Scr facilitated new bone inward growth within bone tunnel and enhanced the bone/iCSP-Scr mechanical interlock, ultimately led to effective tendon graft fixation and promote bone-tendon healing in ACL reconstruction *in vivo*. The pull-out force of the tendon graft from the bone tunnel for the iCSP-Scr group after 14 weeks' ACL construction in the rabbit models was proved even slightly higher than that of Ti screw group. Collectively, the bioactive iCSP-Scr provides a novel and game-changing bone-tendon fixation paradigm facilitating ACL reconstruction, and could be universally expanded to other orthopedic application scenarios. It is also believed that this material design strategy which smartly matched the clinical requirements with the material characteristics will inspire more material innovation in regenerative medicine and other areas.

Ethics approval and consent to participate

All *in vivo* animal experimental procedures were conducted in accordance with Arrive's guidelines and approved by the Institutional Animal Care and Use Committee (IACUC) of Nanfang Hospital (Permit No. IACUC-LAC-20221028-004), and performed according to the Animal Welfare Act and National Institute of Health (NIH) guidelines for the care and use of laboratory animals.

All authors declare that this manuscript is original, has not been published before and is not currently being considered for publication elsewhere. The manuscript has been read and approved by all named authors and all agree with its submission to the journal Bioactive Materials.

CRediT authorship contribution statement

Meihan Tao: Writing – review & editing, Writing – original draft, Visualization, Validation, Software, Resources, Project administration, Methodology, Investigation, Formal analysis, Data curation, Conceptualization. **Zhou Fang:** Methodology. **Yuting Zhu:** Methodology. **Yan Ju:** Methodology. **Zhiguo Hou:** Methodology. **Meimei Fu:** Methodology. **Zhihui Lu:** Validation, Funding acquisition. **Daozhang Cai:** Supervision. **Jian Yang:** Supervision. **Jinshan Guo:** Supervision, Methodology, Funding acquisition, Conceptualization.

Declaration of generative AI and AI-assisted technologies in the writing process

During the preparation of this work, the authors used ChatGPT 3.5 in order to improve language and readability. After using this tool, the authors reviewed and edited the content as needed and take full responsibility for the content of the publication.

Declaration of competing interest

The authors declare that they have no known competing financial interests or personal relationships that could have appeared to influence the work reported in this paper.

Jian Yang is an editor-in-chief for Bioactive Materials and was not involved in the editorial review or the decision to publish this article. All authors declare that there are no competing interests.

Acknowledgements

This work was supported by the Youth Talent of Guangdong Special Support Program (0620220207), the Natural Science Foundation of China (Grant Nos. U21A2099, 82272453, and 82102545), the China Postdoctoral Science Foundation (Grant No. 2022M721515), the Basic and Applied Basic Research Project of Guangzhou City (202201011774), and the Open Program from Guangdong Provincial Key Laboratory of Bone and Joint Degeneration Disease.

Appendix A. Supplementary data

Supplementary data to this article can be found online at https://doi.org/10.1016/j.bioactmat.2024.07.004.

References

[1] T.L. Sanders, H. Maradit Kremers, A.J. Bryan, D.R. Larson, D.L. Dahm, B.A. Levy, M.J. Stuart, A.J. Krych, Incidence of anterior cruciate ligament tears and reconstruction: a 21-year population-based study, Am. J. Sports Med. 44 (6) (2016) 1502–1507, https://doi.org/10.1177/0363546516629944.

[2] B. Patterson, A.G. Culvenor, C.J. Barton, A. Guermazi, J. Stefanik, H.G. Morris, T. S. Whitehead, K.M. Crossley, Poor functional performance 1 year after ACL reconstruction increases the risk of early osteoarthritis progression, Br. J. Sports Med. 54 (9) (2020) 546–553, https://doi.org/10.1136/bjsports-2019-101503.

[3] N. Maniar, M.H. Cole, A.L. Bryant, D.A. Opar, Muscle force contributions to anterior cruciate ligament loading, Sports Med. 52 (8) (2022) 1737–1750, https://doi.org/10.1007/s40279-022-01674-3.

[4] X. He, Y. Li, J. Guo, J. Xu, H. Zu, L. Huang, M. Tim-Yun Ong, P. Shu-Hang Yung, L. Qin, Biomaterials developed for facilitating healing outcome after anterior cruciate ligament reconstruction: efficacy, surgical protocols, and assessments using preclinical animal models, Biomaterials 269 (2021) 120625, https://doi.org/10.1016/j.biomaterials.2020.120625.

[5] T. Zhou, Y. Xu, A. Zhang, L. Zhou, Q. Zhang, Z. Ji, W. Xu, Global research status of anterior cruciate ligament reconstruction: a bibliometric analysis, Efort Open Rev 7 (12) (2022) 808–816, https://doi.org/10.1530/EOR-21-0065.

[6] P.Y. Mengsteab, T. Otsuka, A. McClinton, N.S. Shemshaki, S. Shah, H.M. Kan, E. Obopilwe, A.T. Vella, L.S. Nair, C.T. Laurencin, Mechanically superior matrices promote osteointegration and regeneration of anterior cruciate ligament tissue in rabbits, Proc. Natl. Acad. Sci. U S A 117 (46) (2020) 28655–28666, https://doi.org/10.1073/pnas.2012347117.

[7] T. Lei, T. Zhang, W. Ju, X. Chen, B.C. Heng, W. Shen, Z. Yin, Biomimetic strategies for tendon/ligament-to-bone interface regeneration, Bioact. Mater. 6 (8) (2021) 2491–2510, https://doi.org/10.1016/j.bioactmat.2021.01.022.

[8] R. Yang, G. Li, C. Zhuang, P. Yu, T. Ye, Y. Zhang, P. Shang, J. Huang, M. Cai, L. Wang, W. Cui, L. Deng, Gradient bimetallic ion-based hydrogels for tissue microstructure reconstruction of tendon-to-bone insertion, Sci. Adv. 7 (26) (2021) eabg3816, https://doi.org/10.1126/sciadv.abg3816.

[9] K. Huang, J. Du, J. Xu, C. Wu, C. Chen, S. Chen, T. Zhu, J. Jiang, J. Zhao, Tendon-bone junction healing by injectable bioactive thermo-sensitive hydrogel based on inspiration of tendon-derived stem cells, Mater. Today Chem. 23 (2022) 100720, https://doi.org/10.1016/j.mtchem.2021.100720.

[10] A. Rezansoff, A.D. Firth, D.M. Bryant, R. Litchfield, R.G. McCormack, M. Heard, P. B. MacDonald, T. Spalding, P.C.M. Verdonk, D. Peterson, D. Bardana, A.M. J. Getgood, Anterior cruciate ligament reconstruction plus lateral extra-articular tenodesis has a similar return-to-sport rate to anterior cruciate ligament reconstruction alone but a lower failure rate, Arthroscopy 2 (2023) 384–396, https://doi.org/10.1016/j.arthro.2023.05.019.

[11] R. Papalia, S. Vasta, S. D'Adamio, A. Giacalone, N. Maffulli, V. Denaro, Metallic or bioabsorbable interference screw for graft fixation in anterior cruciate ligament (ACL) reconstruction? Br. Med. Bull. 109 (2014) 19–29, https://doi.org/10.1093/bmb/ldt038.

[12] J. Wang, Y. Wu, H. Li, Y. Liu, X. Bai, W. Chau, Y. Zheng, L. Qin, Magnesium alloy based interference screw developed for ACL reconstruction attenuates peri-tunnel bone loss in rabbits, Biomaterials 157 (2018) 86–97, https://doi.org/10.1016/j.biomaterials.2017.12.007.

[13] P. Kačarević Ž, P. Rider, A. Elad, D. Tadic, D. Rothamel, G. Sauer, F. Bornert, P. Windisch, D.B. Hangyási, B. Molnar, T. Kämmerer, B. Hesse, E. Bortel, M. Bartosch, F. Witte, Biodegradable magnesium fixation screw for barrier membranes used in guided bone regeneration, Bioact. Mater. 14 (2022) 15–30, https://doi.org/10.1016/j.bioactmat.2021.10.036.

[14] X. Qu, H. Yang, B. Jia, M. Wang, B. Yue, Y. Zheng, K. Dai, Zinc alloy-based bone internal fixation screw with antibacterial and anti-osteolytic properties, Bioact. Mater. 6 (12) (2021) 4607–4624, https://doi.org/10.1016/j.bioactmat.2021.05.023.

[15] M. Zhang, T. Gregory, U. Hansen, C.K. Cheng, Effect of stress-shielding-induced bone resorption on glenoid loosening in reverse total shoulder arthroplasty, J. Orthop. Res. 38 (7) (2020) 1566–1574, https://doi.org/10.1002/jor.24711.

[16] D. Zhao, T. Zhu, J. Li, L. Cui, Z. Zhang, X. Zhuang, J. Ding, Poly(lactic-co-glycolic acid)-based composite bone-substitute materials, Bioact. Mater. 6 (2) (2021) 346–360, https://doi.org/10.1016/j.bioactmat.2020.08.016.

[17] C. Zeng, G. Lei, S. Gao, W. Luo, Methods and devices for graft fixation in anterior cruciate ligament reconstruction, Cochrane Database Syst. Rev. 6 (9) (2013) CD010730, https://doi.org/10.1002/14651858.CD010730.

[18] J.F. de Beer, D.N. Bhatia, K.S. van Rooyen, D.F. Du Toit, Arthroscopic debridement and biological resurfacing of the glenoid in glenohumeral arthritis, Knee Surg. Sports Traumatol. Arthrosc. 18 (12) (2010) 1767–1773, https://doi.org/10.1007/s00167-010-1155-8.

[19] J. Wang, J. Xu, X. Wang, L. Sheng, L. Zheng, B. Song, G. Wu, R. Zhang, H. Yao, N. Zheng, M.T. Yun Ong, P.S. Yung, L. Qin, Magnesium-pretreated periosteum for promoting bone-tendon healing after anterior cruciate ligament reconstruction, Biomaterials 268 (2021) 120576, https://doi.org/10.1016/j.biomaterials.2020.120576.

[20] A.T. Hexter, T. Thangarajah, G. Blunn, F.S. Haddad, Biological augmentation of graft healing in anterior cruciate ligament reconstruction: a systematic review, Bone Joint Lett. J 100-b (3) (2018) 271–284, https://doi.org/10.1302/0301-620X.100B3.BJJ-2017-0733.R2.
[21] T. Uno, M. Maruyama, H. Satake, Y. Takakubo, S. Toyono, L. Xing, H. Huang, I. Yuki, A. Suzuki, N. Mura, M. Takagi, Effectiveness of bone marrow-derived platelet-rich fibrin on rotator cuff healing in a rabbit degenerative model, Am. J. Sports Med. 50 (12) (2022) 3341–3354, https://doi.org/10.1177/03635465221116084.
[22] Q. Jiang, L. Wang, Z. Liu, J. Su, Y. Tang, P. Tan, X. Zhu, K. Zhang, X. Ma, J. Jiang, J. Zhao, H. Lin, X. Zhang, Canine ACL reconstruction with an injectable hydroxyapatite/collagen paste for accelerated healing of tendon-bone interface, Bioact. Mater. 20 (2023) 1–15, https://doi.org/10.1016/j.bioactmat.2022.05.003.
[23] L.V. Gulotta, D. Kovacevic, L. Ying, J.R. Ehteshami, S. Montgomery, S.A. Rodeo, Augmentation of tendon-to-bone healing with a magnesium-based bone adhesive, Am. J. Sports Med. 36 (7) (2008) 1290–1297, https://doi.org/10.1177/0363546508314396.
[24] M. Zhang, J. Liu, T. Zhu, H. Le, X. Wang, J. Guo, G. Liu, J. Ding, Functional macromolecular adhesives for bone fracture healing, ACS Appl. Mater. Interfaces 14 (1) (2022) 1–19, https://doi.org/10.1021/acsami.1c17434.
[25] X. Yuan, Y. Zhao, J. Li, X. Chen, Z. Lu, L. Li, J. Guo, Citrate-based mussel-inspired magnesium whitlockite composite adhesives augmented bone-to-tendon healing, J. Mater. Chem. B 9 (39) (2021) 8202–8210, https://doi.org/10.1039/d1tb01710a.
[26] F. Lin, Y.H. Li, W.G. Cui, Injectable hydrogel microspheres in cartilage repair, Biomed, Technol. 1 (2023) 18–29, https://doi.org/10.1016/j.bmt.2022.11.002.
[27] M. Furtado, L. Chen, Z.H. Chen, A. Chen, W.G. Cui, Development of fish collagen in tissue regeneration and drug delivery, Engineered Regen 3 (3) (2022) 217–231, https://doi.org/10.1016/j.engreg.2022.05.002.
[28] Y.J. Zhu, B. Kong, R. Liu, Y.J. Zhao, Developing biomedical engineering technologies for reproductive medicine, Smart Med. 1 (1) (2022), https://doi.org/10.1002/SMMD.20220006.
[29] Y. Zhang, J. Xu, Y.C. Ruan, M.K. Yu, M. O'Laughlin, H. Wise, D. Chen, L. Tian, D. Shi, J. Wang, S. Chen, J.Q. Feng, D.H. Chow, X. Xie, L. Zheng, L. Huang, S. Huang, K. Leung, N. Lu, L. Zhao, H. Li, D. Zhao, X. Guo, K. Chan, F. Witte, H. C. Chan, Y. Zheng, L. Qin, Implant-derived magnesium induces local neuronal production of CGRP to improve bone-fracture healing in rats, Nat. Med. 22 (10) (2016) 1160–1169, https://doi.org/10.1038/nm.4162.
[30] Y. Zhao, J. Li, L. Liu, Y. Wang, Y. Ju, C. Zeng, Z. Lu, D. Xie, J. Guo, Zinc-based tannin-modified composite microparticulate scaffolds with balanced antimicrobial activity and osteogenesis for infected bone defect repair, Adv. Healthc. Mater. 12 (20) (2023) e2300303, https://doi.org/10.1002/adhm.202300303.
[31] J. Guo, X. Tian, D. Xie, K. Rahn, E. Gerhard, M.L. Kuzma, D. Zhou, C. Dong, X. Bai, Z. Lu, J. Yang, Citrate-based tannin-bridged bone composites for lumbar fusion, Adv. Funct. Mater. 30 (27) (2020) 2002438, https://doi.org/10.1002/adfm.202002438.
[32] J. Guo, Z. Xie, R.T. Tran, D. Xie, D. Jin, X. Bai, J. Yang, Click chemistry plays a dual role in biodegradable polymer design, Adv. Mater. 26 (12) (2014) 1906–1911, https://doi.org/10.1002/adma.201305162.
[33] H. Qiu, J. Yang, P. Kodali, J. Koh, G.A. Ameer, A citric acid-based hydroxyapatite composite for orthopedic implants, Biomaterials 27 (34) (2006) 5845–5854, https://doi.org/10.1016/j.biomaterials.2006.07.042.
[34] C. Ma, X. Tian, J.P. Kim, D. Xie, X. Ao, D. Shan, Q. Lin, M.R. Hudock, X. Bai, J. Yang, Citrate-based materials fuel human stem cells by metabonegenic regulation, Proc. Natl. Acad. Sci. U S A 115 (50) (2018) E11741–E11750, https://doi.org/10.1073/pnas.1813000115.
[35] M.E. Mycielska, V.M. Milenkovic, C.H. Wetzel, P. Rümmele, E.K. Geissler, Extracellular citrate in health and disease, Curr. Mol. Med. 15 (10) (2015) 884–891, https://doi.org/10.2174/1566524016666151123104855.
[36] E. Davies, K.H. Müller, W.C. Wong, C.J. Pickard, D.G. Reid, J.N. Skepper, M. J. Duer, Citrate bridges between mineral platelets in bone, Proc. Natl. Acad. Sci. U S A 111 (14) (2014) E1354–E1363, https://doi.org/10.1073/pnas.1315080111.
[37] R.B. Franklin, M. Chellaiah, J. Zou, M.A. Reynolds, L.C. Costello, Evidence that osteoblasts are specialized citrate-producing cells that provide the citrate for incorporation into the structure of bone, Open Bone J. 6 (2014) 1–7, https://doi.org/10.2174/1876525401406010001.
[38] Y. Wang, Y. Zhao, S. Ma, M. Fu, M. Wu, J. Li, K. Wu, X. Zhuang, Z. Lu, J.A.-O. Guo, Injective programmable proanthocyanidin-coordinated zinc-based composite hydrogel for infected bone repair, Adv. Healthc. Mater. 13 (6) (2024) e2302690, https://doi.org/10.1002/adhm.202302690.
[39] W. Zou, J. Dong, Y. Luo, Q. Zhao, T. Xie, Dynamic covalent polymer networks: from old chemistry to modern day innovations, Adv. Mater. 29 (14) (2017).
[40] Y. Liu, Z. Zhang, J. Wang, T. Xie, L. Sun, K. Yang, Z. Li, Renewable tannic acid based self-healing polyurethane with dynamic phenol-carbamate network: simultaneously showing robust mechanical properties, reprocessing ability and shape memory, Polymer 228 (2021) 123860, https://doi.org/10.1016/j.polymer.2021.123860.
[41] S. Zhang, G. Zhao, W. Ma, Y. Song, C. Huang, C. Xie, K. Chen, X. Li, The root-like chitosan nanofiber porous scaffold cross-linked by genipin with type I collagen and its osteoblast compatibility, Carbohydr. Polym. 285 (2022) 119255, https://doi.org/10.1016/j.carbpol.2022.119255.
[42] M. Tao, F. Liang, J. He, W. Ye, R. Javed, W. Wang, T. Yu, J. Fan, X. Tian, X. Wang, W. Hou, Q. Ao, Decellularized tendon matrix membranes prevent post-surgical tendon adhesion and promote functional repair, Acta Biomater. 134 (2021) 160–176, https://doi.org/10.1016/j.actbio.2021.07.038.
[43] M. Tao, T. Ao, X. Mao, X. Yan, R. Javed, W. Hou, Y. Wang, C. Sun, S. Lin, T. Yu, Q. Ao, Sterilization and disinfection methods for decellularized matrix materials: review, consideration and proposal, Bioact. Mater. 6 (9) (2021) 2927–2945, https://doi.org/10.1016/j.bioactmat.2021.02.010.
[44] D. Shan, S.R. Kothapalli, D.J. Ravnic, E. Gerhard, J.P. Kim, J. Guo, C. Ma, J. Guo, L. Gui, L. Sun, D. Lu, J. Yang, Development of citrate-based dual-imaging enabled biodegradable electroactive polymers, Adv. Funct. Mater. 28 (34) (2018) 1801787, https://doi.org/10.1002/adfm.201801787.
[45] M. Wu, Y. Zhao, M. Tao, M. Fu, Y. Wang, Q. Liu, Z. Lu, J. Guo, Malate-based biodegradable scaffolds activate cellular Energetic metabolism for accelerated wound healing, ACS Appl. Mater. Interfaces 15 (44) (2023) 50836–50853, https://doi.org/10.1021/acsami.3c09394.
[46] Z. Zhou, Y. Fan, Y. Jiang, S. Shi, C. Xue, X. Zhao, S. Tan, X. Chen, C. Feng, Y. Zhu, J. Yan, Z. Zhou, Y. Zhao, J. Liu, F. Chen, S. He, Mineralized enzyme-based biomaterials with superior bioactivities for bone regeneration, ACS Appl. Mater. Interfaces 14 (32) (2022) 36315–36330, https://doi.org/10.1021/acsami.2c05794.
[47] N. Monteiro, D. Ribeiro, A. Martins, S. Faria, N.A. Fonseca, J.N. Moreira, R.L. Reis, N.M. Neves, Instructive nanofibrous scaffold comprising runt-related transcription factor 2 gene delivery for bone tissue engineering, ACS Nano 8 (8) (2014) 8082–8094, https://doi.org/10.1021/nn5021049.
[48] Y. Chen, S. Yang, S. Lovisa, C.G. Ambrose, K.M. McAndrews, H. Sugimoto, R. Kalluri, Type-I collagen produced by distinct fibroblast lineages reveals specific function during embryogenesis and osteogenesis imperfecta, Nat. Commun. 12 (1) (2021) 7199, https://doi.org/10.1038/s41467-021-27563-3.
[49] T. Sakabe, K. Sakai, T. Maeda, A. Sunaga, N. Furuta, R. Schweitzer, T. Sasaki, T. Sakai, Transcription factor scleraxis vitally contributes to progenitor lineage direction in wound healing of adult tendon in mice, J. Biol. Chem. 293 (16) (2018) 5766–5780, https://doi.org/10.1074/jbc.RA118.001987.
[50] T.A. Järvinen, L. Józsa, P. Kannus, T.L. Järvinen, T. Hurme, M. Kvist, M. Pelto-Huikko, H. Kalimo, M. Järvinen, Mechanical loading regulates the expression of tenascin-C in the myotendinous junction and tendon but does not induce de novo synthesis in the skeletal muscle, J. Cell Sci. 116 (Pt 5) (2003) 857–866, https://doi.org/10.1242/jcs.00303.
[51] S. Dex, P. Alberton, L. Willkomm, T. Söllradl, S. Bago, S. Milz, M. Shakibaei, A. Ignatius, W. Bloch, H. Clausen-Schaumann, C. Shukunami, M. Schieker, D. Docheva, Tenomodulin is required for tendon endurance running and collagen I fibril adaptation to mechanical load, EBioMedicine 20 (2017) 240–254, https://doi.org/10.1016/j.ebiom.2017.05.003.
[52] M. Schneider, P. Angele, T.A.H. Järvinen, D. Docheva, Rescue plan for Achilles: Therapeutics steering the fate and functions of stem cells in tendon wound healing, Adv. Drug Deliv. Rev. 129 (2018) 352–375, https://doi.org/10.1016/j.addr.2017.12.016.
[53] J.Y. Li, E.H. Pow, L.W. Zheng, L. Ma, D.L. Kwong, L.K. Cheung, Quantitative analysis of titanium-induced artifacts and correlated factors during micro-CT scanning, Clin. Oral Implants Res. 25 (4) (2014) 506–510, https://doi.org/10.1111/clr.12200.